

# 6

## EFFECT MODELS FOR CONSEQUENCE ANALYSIS

*“Every cause must produce an effect and every effect must have a cause”*

*Law of Universal Causation in Logic*

We discussed in Chapter 5 that there are two components to consequence modelling—effects models and vulnerability models. This chapter deals with the physical effects of releases of hazardous materials and the subsequent events that generate thermal radiation, toxic gas concentrations or explosion overpressures. Vulnerability of receptors is dealt with in Chapter 7. Wells (1980) has described a number of issues of how to incorporate the effects and vulnerability modelling in process plant design.

It is not the purpose of this chapter to give a complete coverage of effect models. The chapter provides an overview of the key issues and approaches, providing references for more detailed modelling information. What is given are insights and suggestions for the use of such models in hazard analysis. A number of well established software tools are available for these predictions.

### 6.1 RELEASE OF HAZARDOUS SUBSTANCES

#### 6.1.1 Factors Affecting Release Modelling

The first category of events is the release of a hazardous material from containment such as a pipe, tank and vessel or transport tanker.

Table 6-1 gives a summary of the types and location of releases (Lees, 2001) which could be encountered. Each release has a specific characteristic which is dependent on

- (i) the physical state of the material (solid, liquid, gas)
- (ii) the physical situation (pipe, pump, vessel)
- (iii) physico-chemical properties (density, viscosity, vapour pressure, reactivity)
- (iv) operating conditions (pressure, temperature, concentration)

Variations in factors such as aperture size, type of plant, material state lead to quite different release cases. Taking one item from each parameter in Table 6-1, a large number of combinations is possible.

Some simple models can help quantify the release rates. What follows is a summary of some simple models and examples of their application.

**TABLE 6-1 RELEASE CASES**

FLUID:	ENCLOSURE:
<ul style="list-style-type: none"> <li>• gas/vapour</li> <li>• liquid</li> <li>• two-phase</li> </ul>	<ul style="list-style-type: none"> <li>• inside building</li> <li>• in open air</li> </ul>
PLANT:	HEIGHT:
<ul style="list-style-type: none"> <li>• vessel</li> <li>• other equipment</li> <li>• pipework</li> </ul>	<ul style="list-style-type: none"> <li>• below ground level</li> <li>• at ground level</li> <li>• above ground level</li> </ul>
APERTURE:	FLUID MOMENTUM:
<ul style="list-style-type: none"> <li>• complete rupture</li> <li>• limited rupture</li> </ul>	<ul style="list-style-type: none"> <li>• low</li> <li>• high</li> </ul>

### 6.1.2 Key Points in Release Modelling

It cannot be over-emphasized that release modelling or “source” modelling is one of the most important aspects of consequence analysis. It is the first event in any incident and as such plays a dominant role in the outcomes. Key issues in dealing with releases include:

(i) **Material state:**

A single component or mixture can, under appropriate conditions, exist in several states such as vapour, liquid or solid. It is vital that the storage conditions (temperature and pressure) are considered, so as to determine the form of release.

In storage vessels containing liquids, material can escape from either the vapour space or in the liquid region, having significantly different release rates and subsequent behaviour.

(ii) **System dynamics:**

Most releases are dynamic (time variant) in nature, since temperatures and pressures within a containment system change as inventory changes or as the release continues.

Pressurized gas storage vessels drop in pressure as gas is released. This rate of pressure decrease is dependent on the size of the failure. This in turn reduces the driving force (pressure difference) and hence the flowrates over time. Basing the discharge rates only on initial system conditions can lead to massive conservatism in consequence analysis.

Similar comments can be made when considering releases from major gas transmission lines, where rapid depressurization can occur depending on the aperture size of the failure. Here the initial gas “burst” rate can rapidly diminish in seconds as the depressurization takes place.

(iii) **Isolatable Inventory:**

In process plants, a frequently encountered situation is where safety instrumented systems (SIS) activate in order to isolate an inventory.

In such a case, the maximum release quantity is restricted to the inventory isolated from other process units. The time-variant release rate and the duration of the release need to be evaluated for effects modelling.

(iv) **Flow systems:**

In many cases, release events occur in piping systems where the flow is maintained by a pump or a gas compressor. In these instances, if the motive device continues to operate, then the sustained flow is ultimately controlled by the following:

- (a) Aperture size controlling. The leak rate is much smaller than the process flow rate, and the release rate is controlled by the aperture size of the leak.
- (b) Process flow rate controlling. The line or vessel failure is substantial, and after an initial high rate of release, the release rate would settle down to the process flow rate until the motive device is shut down.

(v) **Physico-chemical phenomena:**

Substances and mixtures can often display unexpected behaviour due to the phase equilibria properties. Substances such as acetic acid can form dimers (double molecules) in the vapour phase. Hydrogen fluoride (HF) forms oligomers (multiple molecules). This type of chemical and phase behaviour directly affects estimates of release rates.

Some materials such as gases compressed into liquid form, such as LPG, butane or butadiene produce vapour-liquid mixtures on release from containment. The subsequent behaviour of the release then needs to be handled correctly to estimate vapour and liquid source terms from such “flashing” releases. “Rain-out” of liquid droplets can also occur.

(vi) **Release location:**

The release behaviour depends on the location in the system and the presence of nearby obstacles or equipment. Key issues to consider are:

- Direct discharge impingement altering the ultimate release orientation. For example, to ground or onto nearby structures.
- Release on suction or discharge side of pumps or compressors.
- Release inside, outside or over banded/diked areas.
- Release from vessel wall, nozzle or along connecting pipework in the case of “flashing” liquids, can give different release rates, based on the length of the leak path.

#### EXAMPLE 6-1 GAS TRANSMISSION LINE RELEASE

Figure 6-1 shows gas release estimates for the full-bore discharge from a natural gas pipeline of 457 mm diameter operating at 15.3 MPa. Rapid depressurization leads to a significant drop in gas discharge rate over the first 10 seconds.

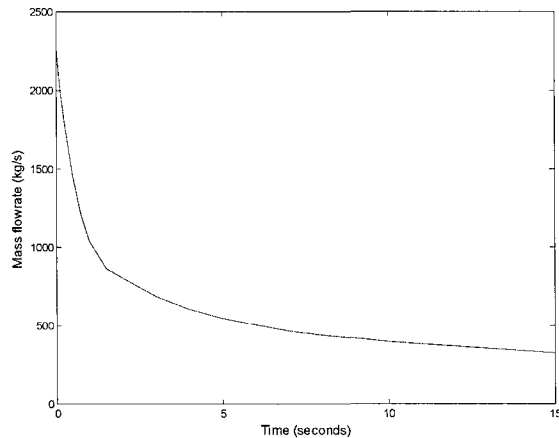


FIGURE 6-1 GAS RELEASE FLOW TRANSIENT FOR PIPELINE

## 6.2 GAS RELEASES

Figure 6-2 gives an overview of gas release types and potential consequences. Both short-term and continuous releases are covered as well as subsequent impacts. In considering gas releases, there are two situations which need to be addressed. The first is when the pressure driving force ( $P_1 - P_2$ ) is small and the gas flowrate is below sonic velocity (speed of sound). The other is when the pressure difference is

large when there is sonic flow. There is a critical pressure ratio  $\left(\frac{P_2}{P_1}\right)$  which

determines the type of release, where  $P_1$  is the upstream (higher) pressure and  $P_2$  refers to the downstream (lower) pressure. Sonic flows occur when this ratio is less than about 0.5.

In some cases, the flowrate switches from sonic to subsonic flow as  $P_1$  decreases and the critical pressure ratio is reached.

Table 6-2 gives the common models for pressurized gas releases.

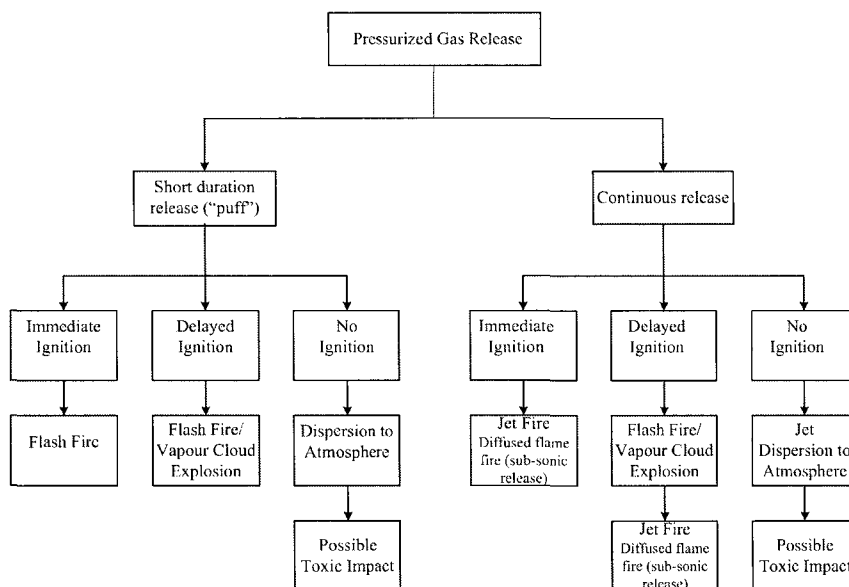


**FIGURE 6-2 PRESSURIZED GAS RELEASE CONSEQUENCES**

**TABLE 6-2 GAS DISCHARGE MODELS**

The specific discharge rates for gases are given by the following models, where the high pressure is condition 1, the low pressure is condition 2.

Subsonic Flow

$$W = \frac{C_d}{V_2} \left[ 2P_1 V_1 \frac{k}{k-1} \left( 1 - \left( \frac{P_2}{P_1} \right)^{\frac{k-1}{k}} \right) \right]^{\frac{1}{2}} \quad (6.1)$$

Sonic Flow

$$W = C_d \left[ \frac{P_1}{V_1} k \left( \frac{2}{k+1} \right)^{\frac{k+1}{k-1}} \right]^{\frac{1}{2}} \quad (6.2)$$

where:

- $W$  = specific mass flowrate (kg/m<sup>2</sup>s)
- $k$  = ratio of specific heats  $C_p/C_v$ 
  - ≈ 1.67 for monatomic gases (argon, helium)
  - ≈ 1.41 for diatomic gases (O<sub>2</sub>, N<sub>2</sub>, H<sub>2</sub>)
  - ≈ 1.3 for complex gases (CH<sub>4</sub>, CO<sub>2</sub>)
- $V_1, V_2$  = specific volumes of gases at conditions 1 and 2 (m<sup>3</sup>/kg)
- $P_1$  = upstream (high) pressure (Pa)
- $P_2$  = downstream (low) pressure (Pa)
- $C_d$  = discharge coefficient
  - ~ 0.61 for sharp discharge hole
  - ~ 0.80 for smooth discharge hole

The critical pressure ratio for sonic conditions is given by:

$$\frac{P_2}{P_1} < \left( \frac{2}{k+1} \right)^{\frac{k}{k-1}} \quad (6.3)$$

#### EXAMPLE 6-2 DISCHARGE OF ETHYLAMINE VAPOUR

The gas release from a broken 25mm nozzle in the vapour space of a storage tank is required. Storage temperature is 65°C giving a 500 kPa vapour pressure. Specific volume of gas is 0.125 m<sup>3</sup>/kg.

From equation (6.3) the critical pressure ratio is:

$$\frac{P_2}{P_1} = \left( \frac{2}{k+1} \right)^{\frac{k}{k-1}} \simeq \left( \frac{2}{1.3+1} \right)^{\frac{1.3}{0.3}} = 0.55$$

Since  $P_2/P_1 < 0.55$  sonic flow occurs. Equation (6.2) gives:

$$W = 0.6 \left[ \frac{5 \times 10^5}{0.125} (1.3) \left( \frac{2}{2.3} \right)^{\frac{2.3}{0.3}} \right]^{\frac{1}{2}} = 800 \text{ kg/m}^2\text{s}$$

Mass flowrate  $G = W \times \text{Area of flow} = 800 (4.91 \times 10^{-4}) = 0.4 \text{ kg/s}$

Figure 6-3 summarises the sequence of effects following a gas release.

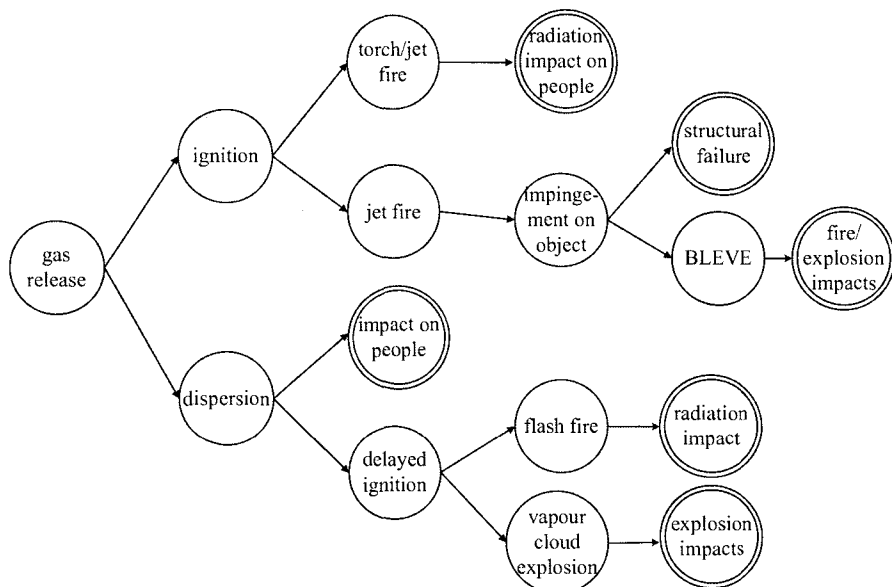


FIGURE 6-3 LIKELY GAS RELEASE INCIDENTS

## 6.3 LIQUID RELEASES

### 6.3.1 Atmospheric Storage

Many liquids are stored in tanks vented to atmosphere. Leaks from such storage facilities are driven by the available head of liquid, which generates the internal pressure at the leak aperture. The rate is a function of the pressure and the aperture size as well as fluid density. Leaks from bunded/diked storage can end up in the containment area. For atmospheric storage, bund/dike design and distance of bund wall to tank is specified by codes (e.g. NFPA30-2000, AS1940-1993) to ensure that jets of liquid cannot project over bunds or dikes.

### 6.3.2 Pressurized Storage

When a liquid is released under pressure it flows at a rate which is dependent on the pressure difference across the hole (aperture) and the size of the hole. Figure 6-4 shows the various incidents that can take place on the release of liquids from containment.

When release is from pressurized storage there are two contributions to the pressure driving the liquid from the hole. The first is the pressure in the tank due to pressurized storage. The second is the liquid head generated by the height of liquid above the hole. In pipelines we are normally given an operating pressure and hence the second term is not relevant to the flowrate calculation.

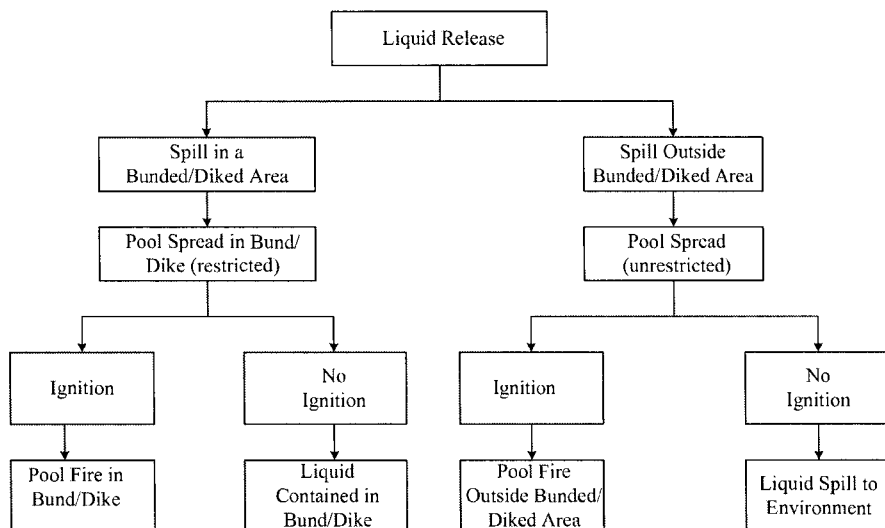


**FIGURE 6-4 CONSEQUENCES OF LIQUID RELEASE FROM STORAGE**

Table 6-3 gives the model used for estimating liquid releases, based on the Bernoulli equation.

**TABLE 6-3 LIQUID DISCHARGE MODEL**

The discharge rate is given by:

$$W = C_d \sqrt{2\rho_L(P_1 - P_2)} + C_d \rho_L \sqrt{2gh} \quad (6.4)$$

where:

$W$	= specific mass flowrate (kg/m <sup>2</sup> s)
$\rho_L$	= liquid density (kg/m <sup>3</sup> )
$C_d$	= discharge coefficient 0.61 sharp edged orifice 0.80 short piece of pipe
$P_1$	= upstream absolute pressure (Pa)
$P_2$	= downstream absolute pressure (Pa)
$h$	= head of liquid (m)
$g$	= gravitational constant (9.81 m/s <sup>2</sup> )

We calculate the mass flowrate per unit area ( $W$ ) then multiply by the area of the opening to get the final mass flowrate.

#### **EXAMPLE 6-3 DISCHARGE OF ETHYLAMINE FROM A FUEL STORAGE VESSEL**

A 3.0 m high tank has a leak via a broken 25mm nozzle on its base. Storage temperature is 65°C and the vapour pressure of the liquid is  $5 \times 10^5$  Pa. Liquid density is 680 kg/m<sup>3</sup>, and atmospheric pressure is  $1 \times 10^5$  Pa.

Using equation (6.4) we have:

$$W = 0.61\sqrt{2(680)(5 \times 10^5 - 1 \times 10^5)} + 0.61(680)\sqrt{2(9.81)3.0} = 17409 \text{ kg/m}^2\text{s}$$

$$\text{Area of aperture} = \pi D^2/4, \text{ hence } A = \frac{\pi}{4}(0.025)^2 = 4.91 \times 10^{-4} \text{ m}^2$$

■ ■ ■

$$\text{Mass flow } G = W.A = 8.5 \text{ kg/s}$$

Figure 6-5 is a summary of the sequence of effects following a liquid release.



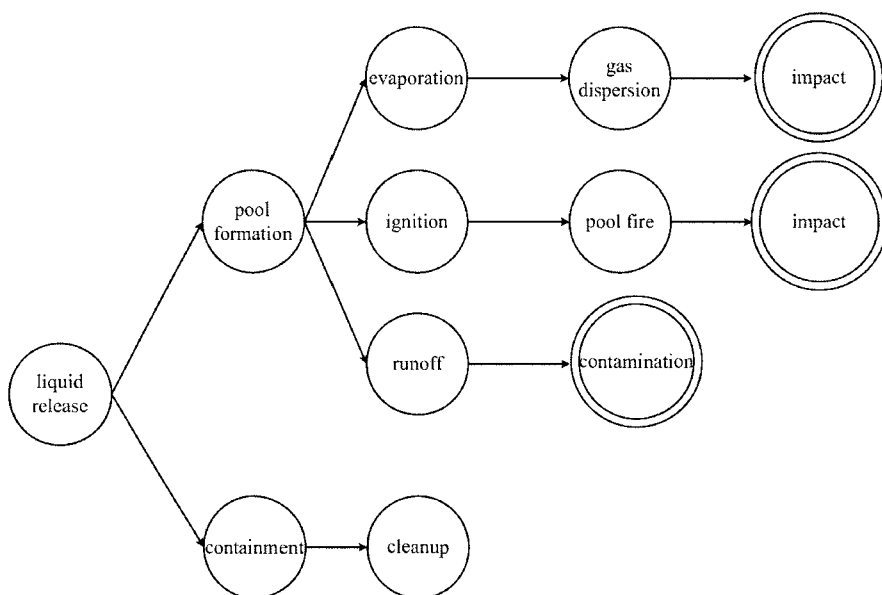


FIGURE 6-5 LIKELY LIQUID RELEASE SCENARIOS

## 6.4 FLASHING LIQUID RELEASES

### 6.4.1 Liquefied Gases

Liquefied gases are common substances. Many gases are liquefied by two mechanisms:

- (i) Liquefaction by pressure, such as propane or butane (LPG)
- (ii) Liquefaction by cooling, such as ethylene

Liquefaction reduces the volume of the material and aids in storage and handling. It does however generate significant effects when loss of containment occurs. The following sections outline the important issues.

### 6.4.2 Liquids above their Atmospheric Boiling Point

Liquefied gas releases are common and pose particular problems due to the “flashing” nature of the liquid as the pressure is reduced. Figure 6-6 shows the potential incidents associated with liquefied gas releases. In some cases, like the storage of LPG under pressure, when the liquid LPG starts to flow down a pipe which has a hole in it, there is a significant pressure gradient along the leak path, from storage pressure to the “choke” pressure (i.e. pressure at the hole at the point of discharge to atmosphere). This causes part of the LPG to vaporize, and a two-phase mixture exists at the choke. Thus the discharge is a mixture of both liquid and vapour.

The release rate for such a flow is given in Table 6-4.

TABLE 6-4 TWO PHASE FLOW RELEASE MODEL

The specific mass flowrate is given by:

$$W = C_d \sqrt{2\hat{\rho}(P_1 - P_c)} \quad (6.5)$$

where:

- $C_d \cong 0.61$   
 $\hat{\rho}$  = mean density of the vapour-liquid mixture ( $\text{kg/m}^3$ )  
 $P_1$  = upstream pressure (Pa)  
 $P_c$  = choke pressure (Pa)

We calculate the mass flowrate per unit area ( $W$ ) then multiply by the area of the opening to get the final mass flowrate.

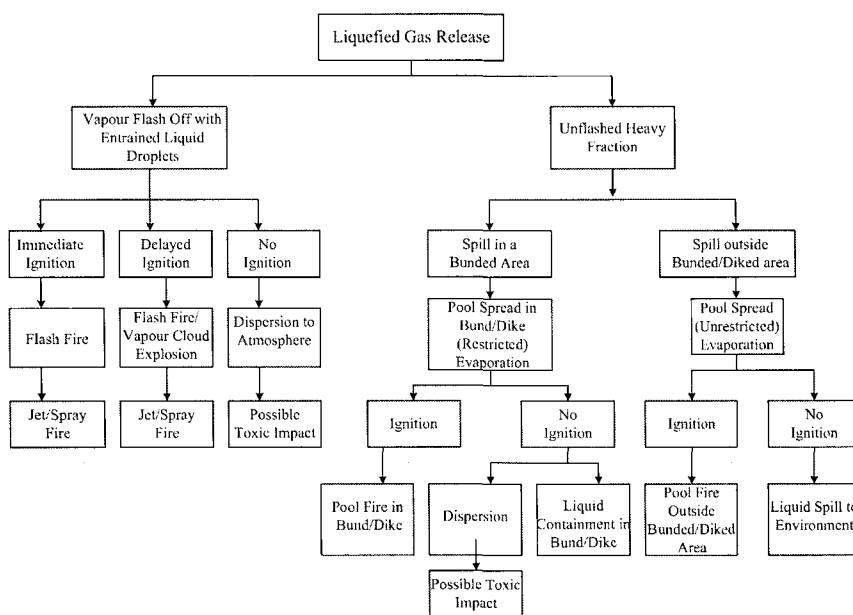


FIGURE 6-6 CONSEQUENCE OF RELEASE OF LIQUEFIED GASES

In equation (6.5) the choke pressure  $P_c$  is difficult to estimate and is clearly critical in determining the specific mass flowrate  $W$ . This is because the temperature and hence fluid properties change along the pipe thus making the calculation non-trivial. Techniques are available to handle this situation in a thermodynamically rigorous manner (TNO 1997).

An alternate approach suggested by Fletcher and Johnson (1984) uses a simpler expression:

$$W = C_d f(l) \sqrt{P_1} \quad (6.6)$$

where:

- $W$  = specific mass flowrate ( $\text{kg/m}^2\cdot\text{s}$ )
- $f(l)$  = flow correction function, based on length
- $C_d$   $\cong 0.61$
- $P_1$  = upstream pressure (Pa)

The function  $f(l)$  is derived from experiments with 2-phase water flows and varies with length of pipe ( $l$ ) to the break. The following table presents values of  $f(l)$  as a function of distance to the break.

**TABLE 6-5 FLOW CORRECTION FACTORS FOR 2-PHASE FLOW**

Length to aperture $l(\text{mm})$	$f(l)$
0	44.72
25	31.62
50	22.36
75	18.71
100	17.32
150	16.12
200	15.81
300	15.49
500	15.33
700	14.14

It should be remembered that this is an approximate method, which nevertheless gives a reasonable first estimate of the flow. Use of this method should be restricted to pipe lengths no greater than 750 mm, e.g. pipework close to storage vessels. Other techniques are needed for long pipes such as LPG transmission systems.

#### EXAMPLE 6-4 ESCAPE OF ETHYLAMINE IN CONNECTING PIPE

Consider a release of ethylamine from a 25 mm diameter pipe connected to the base of a storage tank, where ethylamine is stored at  $65^\circ\text{C}$  and a vapour pressure of  $5 \times 10^5$  Pa. Liquid density is  $680 \text{ kg/m}^3$ .

The pipe is broken 500 mm from where it joins the tank. The height of liquid in the tank is 3 metres.

The pressure at the tank base ( $P_1$ ), is the vapour pressure plus the liquid head:

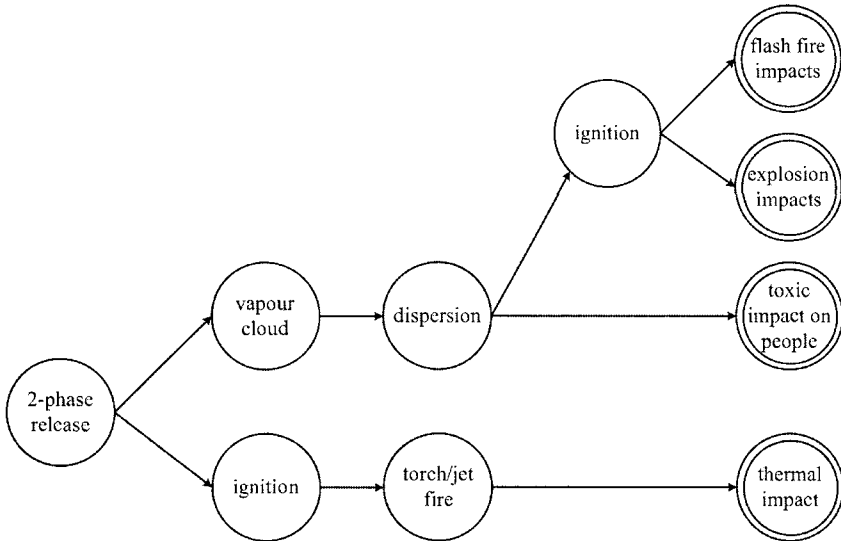
$$P_1 = 5 \times 10^5 + \rho_L gh = 5 \times 10^5 + 680(9.81)(3) = 5.2 \times 10^5 \text{ Pa}$$

Using the simplified equation (6.6) and the flow correction from Table 6-5:

$$W = 0.61(15.3)\sqrt{5.2 \times 10^5} = 6743 \text{ kg/m}^2\text{s}$$

The mass flowrate is then

■ ■ ■  $G = W.(Area) = 6743 (4.91 \times 10^{-4}) = 3.3 \text{ kg/s}$



■ ■ ■ FIGURE 6-7 TWO-PHASE RELEASE INCIDENTS

### 6.4.3 Flash-off and Rainout

When a liquid held under pressure and at a temperature above its normal boiling point is released, some of the liquid “flashes” to form vapour. In these cases it is important to know how much vapour is formed. Not only is vapour formed but droplets of liquid are entrained in the vapour. Drops of very small size (aerosol) subsequently form part of the vapour cloud. Larger droplets may “rain out” and drop back to ground. This mechanism needs to be considered in effects modelling. Table 6-6 gives the model for computing the flashed amount from pressurized release. This is derived from an energy balance on the liquid.

TABLE 6-6 FLASH MODEL FOR LIQUEFIED GASES

The mass fraction of liquid flashed ( $\phi$ ) is:

$$\phi = 1 - \exp \left[ -\frac{C_p}{\Delta H_v} (\theta_1 - \theta_2) \right] ; \quad \theta_1 > \theta_2 \quad (6.7)$$

where:

$C_p$	= specific heat of liquid (kJ/kgK)
$\Delta H_v$	= latent heat at boiling point (kJ/kg)
$\theta_1$	= storage temperature (K)
$\theta_2$	= normal boiling point (K)

Typically the fraction entrained ( $e$ ) is:  $e = \phi$  (if  $\phi < 0.5$ ) or  $e = 1 - \phi$  (if  $\phi > 0.5$ )

Total mass of cloud is:  $W = (e + \phi) W_o$  (6.8)

Volume of cloud is:  $V = \frac{WM_a}{\rho_a M}$  (6.9)

where:

$\rho_a$	= density of air (kg/m <sup>3</sup> )
$M_a$	= molecular weight of air (29 kg/kgmole)
$M$	= molecular weight of fluid (kg/kgmole)
$V$	= volume of cloud (m <sup>3</sup> )
$W$	= cloud mass (kg)
$W_o$	= initial mass of liquid (kg)

#### EXAMPLE 6-5 PRESSURE RELEASE OF STORAGE TANK

Pressure is suddenly reduced on a tank of ethylamine via a significant structural failure which leads to release of the contents. The basic data are:

$C_p$	= 2.92 kJ/kgK
$\theta_1$	= initial temperature = 65 + 273 = 338K
$\theta_2$	= boiling point = 290K
$\Delta H_v$	= 623 kJ/kg

Using equation (6.7) the flashed fraction is

$$\phi = 1 - \exp \left[ -\frac{2.92}{623} (338 - 290) \right] = 0.20$$

Spray fraction:  $e \cong \phi = 0.2$  (since  $\phi < 0.5$ )

Fraction of vapour is  $\phi + e \cong 0.4$

If the tank contained 20,000 kg of ethylamine then the mass of material in the cloud is approximately:

■ ■ ■

$$W = 0.4 (20,000) = 8000 \text{ kg.}$$

## 6.5 EVAPORATION OF LIQUID POOLS

When a liquid is spilled and there is air movement over the surface, the substance will evaporate and travel downwind. It is necessary to know the rate at which material evaporates as this can then be used with a dispersion model to calculate downwind distances to flammability limits or specified toxic gas concentrations.

The principal factors requiring consideration in treating evaporation from liquid pools are given in Table 6-7.

TABLE 6-7 KEY FACTORS IN EVAPORATION MODELS

- Pool extent: contained or unrestrained spread
- Ground conditions: porous, non-porous, ...
- Ambient conditions: windspeed, temperature, cloud cover
- Evaporation regime: non-boiling, boiling pools
- Heat transfer: solar, ground effects, ambient, ...
- Physico-chemical properties: vapour pressure, boiling point, ...
- Mass transfer: convective, stagnant film (no wind)
- Time effects: transient, steady state

Figure 6-8 shows a typical scenario for contained spills and the various heat and mass transfer mechanisms that can be important. Table 6-8 develops a generic pool evaporation model.

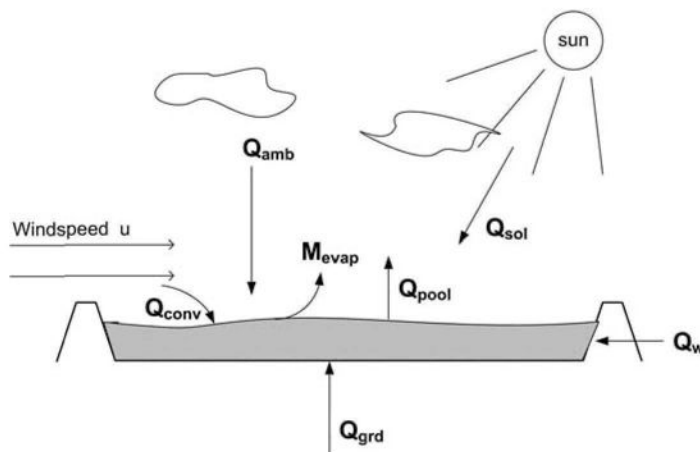


FIGURE 6-8 POOL EVAPORATION - KEY MECHANISMS

TABLE 6-8 GENERIC POOL EVAPORATION MODEL

A general dynamic model can be developed which accounts for these controlling factors (Kawamura and Mackay 1987).

This is an energy balance that can be written as:

$$\frac{dE_p}{dt} = \frac{d(M_p T_p C_p)}{dt} = Q_{amb} + Q_{conv} + Q_{grd} + Q_w + Q_{sol} - Q_{pool} - \dot{m} A \Delta H_v \quad (6.10)$$

where:

$E_p$	= total pool energy (kW)
$M_p$	= mass of liquid in the pool (kg)
$T_p$	= pool temperature (K)
$C_p$	= liquid heat capacity (kJ/kgK)
$Q_{amb}$	= longwave radiation from atmosphere (kW)
$Q_{conv}$	= convective heat flux from wind (kW)
$Q_{grd}$	= conductive heat flow from ground (kW)
$Q_w$	= conductive heat flow from walls (kW)
$Q_{sol}$	= shortwave solar radiation (kW)
$Q_{pool}$	= longwave radiation from the pool (kW)
$\dot{m}$	= evaporation rate (kg/s.m <sup>2</sup> )
$A$	= pool surface area (m <sup>2</sup> )
$\Delta H_v$	= latent heat at boiling point (kJ/kg)

Correlations for the  $Q$  terms can be obtained in standard references (TNO 1997) whilst mass transfer coefficients from pools are also available (Kawamura and Mackay 1987). The Kawamura correlation is:

$$k_m = 4.786 \times 10^{-3} u_w^{0.78} d_p^{-0.11} Sc^{-0.67} \quad (6.11)$$

Here the Schmidt number ( $Sc$ ) =  $\nu_a/D_a$  ( $\sim 0.8$  for vapours)

and

$\nu_a$	= vapour kinematic viscosity (m <sup>2</sup> /s)
$D_a$	= diffusivity of vapour in air (m <sup>2</sup> /s)
$d_p$	= pool diameter (m)
$u_w$	= wind velocity (m/s)
$k_m$	= mass transfer coefficient (m/s)

Other issues that often need addressing in pool evaporation events are:

- (i) The prediction of pool spread if the release is outside bunded/diked areas. This is typically in the form of:

$$r(t) \cong ct^b \quad (6.12)$$

where  $C$  and  $b$  are constants relevant to particular release and ground conditions.

- (ii) Ground cooling under the pool. Here a hot ground surface may cool rapidly on contact with the liquid and thus  $Q_{grd}$  might reduce rapidly, especially for cryogenic liquid spills.
- (iii) Boiling pools. In the case where liquefied gas is released to ground the evaporative mechanism is controlled by boiling. This requires an estimate of critical heat fluxes. Models such as LPOOL (Cavanaugh et al. 1994) consider this mechanism. In the case of LPOOL, initial flash and aerosol entrainment models are also available.

In most models, the evaporation rate for non-boiling pools is a function of  $u_w^{0.78}$ , reflecting the 0.78 power dependence within the mass transfer correlation. In many cases, initial evaporation estimates based on steady state conditions can be given by rather simple correlations. The evaporation rate models by Lees (1980) and Peress (2003) are given in Table 6-9.

**TABLE 6-9 SIMPLE EVAPORATION MODELS**

The evaporation rate from small rectangular and circular pools is given by (Lees, 1980) as:

Rectangular Pools:

$$E_R = 2.625 \times 10^{-7} \left( \frac{M.P^\circ}{T} \right) u_w^{0.78} x^{0.89} y \quad (6.13)$$

Circular Pools:

$$E_C = 7.876 \times 10^{-7} \left( \frac{M.P^\circ}{T} \right) u_w^{0.78} r^{1.89} \quad (6.14)$$

where:

$E_R, E_C$	= evaporation rate (kg/s)
$x$	= downwind pool dimension (m)
$y$	= crosswind pool dimension (m)
$M$	= molecular weight of liquid (kg/kgmole)
$P^\circ$	= vapour pressure of the liquid (Pa)
$T$	= absolute temperature of liquid (K)
$u_w$	= mean wind speed (m/s)
$r$	= radius of pool (m)

The model by Peress (2003) in SI units is given by:

$$E_p = 2.117 \times 10^{-6} u^{0.78} M^{\frac{2}{3}} \cdot \frac{AP^\circ}{T} \quad (6.15)$$

where  $A$  = pool area (m<sup>2</sup>)



Where actual experimental data exists for pool evaporation rate, this should be used in preference to the models. Shaw and Briscoe (1978) describe the pool evaporation rates for specific substances including LNG.

#### EXAMPLE 6-6 EVAPORATION OF ETHYLAMINE

A rectangular pool of ethylamine is formed which has dimensions 2m wide and 4m long in the direction of the wind which is blowing at 2 m/s. What is the evaporation rate if the liquid is at an ambient temperature of 15°C?

Data: Molecular weight = 45.085 kg/kmol  
Antoine vapour pressure equation for ethylamine is:

$$\ln(P^\circ) = 17.0073 - \frac{2616.73}{(T - 37.3)}$$

where  $P^\circ$  = mmHg, T = Kelvin

Now at 15°C, T = 273.15 + 15 = 288K so that,

$$\ln(P^\circ) = 17.0073 - \frac{2616.73}{(288 - 37.3)} = 717.6 \text{ mmHg} \equiv 95664 \text{ Pa}$$

Using the evaporation equation (6.13) for  $E_R$

$$E_R = 2.625 \times 10^{-7} \left[ \frac{45.085(95664)}{288} \right] (2)^{0.78} (4)^{0.89} (2) = 0.046 \text{ kg/s}$$

Using the Peress equation (6.15) we obtain:

$$E_P = 2.117 \times 10^{-6} (2)^{0.78} (45.09)^{\frac{2}{3}} \frac{8(95664)}{288} = 0.112 \text{ kg/s}$$

Hence there is a variability factor of 3 in the results from the 2 methods. If critical then more sophisticated methods such as the LPOOL model should be used.

### 6.5.1 Estimation of Release Duration

The duration of a release is critical in determining the ultimate effects from many release events. In many cases, release duration is not continuous and steady, so that assumptions need to be incorporated into the release events. Such issues include:

- (i) The short term release of materials from relief devices such as pressure relief valves.

- (ii) The varying release of liquids and gases from pipelines and vessels that are being depressurized by the release.
- (iii) The limitation of release amounts due to inventories in the system.
- (iv) The limitation of release duration by the activation of emergency isolation systems such as emergency shutdown (ESD) devices.
- (v) The intervention of operational personnel in limiting release durations through manual isolation or other controls.

In many cases, where the release rate and duration are critical factors, dynamic models can be employed to obtain time varying estimates that are closer to reality. Continuous, maximum flow assumptions can lead to significant conservatism.

## 6.6 EFFECTS MODELLING OF FIRE

The key physical parameter associated with fires is the thermal radiation intensity. This is normally stated in kilowatts per square metre ( $\text{kW/m}^2$ ). Various levels of radiation intensity can have differing effects. On humans the effects range from skin burns to fatality. On structures fire impact can result in loss of mechanical integrity and load bearing capacity. A summary of radiation intensity values and their effects is provided in Chapter 7 (Table 7-1).

In planning and design of activities where flammable substances are present, it is required to evaluate potential radiation intensities from various fire incidents such as flash fires, jet or torch fires, pool fires and BLEVEs. Each fire event has particular characteristics which need to be appreciated in order to evaluate fire radiation intensities. The following sections deal with the key fire scenarios often encountered in the process industries. Much research has been conducted into fires and reported in the literature (Crowley and Johnson 1992, 1992a, 1992b) and the Fire and Blast Information Group (FABIG) of the Steel Construction Institute (1998) for offshore topside structures.

The following sections outline simple approaches to estimating radiation intensities for each of these events.

### 6.6.1 Fires on Pools

In the following sections the key characteristics of pool fires that affect potential impacts are discussed. In many cases, uncertainties in regard to parameters such as emissive power, wind effects and burning rates can be investigated using sensitivity studies (see section 5.2.2.2).

#### 6.6.1.1 *Characteristics of pool fires*

Pool fires are one of the most common occurrences in the process industries. Many occur because of accidental releases of flammable material from storage or in transport situations. The spilled material can be contained in diked or bunded areas or some cases flows unimpeded across land or into drainage areas.

Pool fires are primarily characterized by the heat of combustion and how that is distributed into radiative, convective and reflective components. Convection

leads to high heat releases in the plume whilst radiant energy impacts nearby structures or people. The reflective or feedback heat aids liquid vaporization (Hamins et al. 1995).

Pool fires are characterized by varying levels of thermal radiation that are dependent on the flammable material. The surface emissive radiation flux ( $\text{kW/m}^2$ ) is highly dependent on the flammable material, the size of the fire, which determines the effectiveness of combustion air ingress, and the prevailing wind conditions. The most prominent factor is the area of the fire which determines flame size. The ratio of carbon to hydrogen (C:H) in the flammable substance determines the surface emissive power of the flame. High C:H ratio substances typically burn with smoky flames compared with low C:H ratio materials.

It is important to recognize that there are 3 main zones in a pool fire (Hamins et al. 1995):

- (i) Fuel rich zone:  
located just above the liquid pool, this is roughly 20% of the flame height. Here, little air (oxygen) has penetrated. The flame is usually quite bright with little smoky component.
- (ii) Intermittent zone:  
where the majority of the combustion takes place as air mixes with the hydrocarbons. Here combustion products such as carbon monoxide (CO), carbon dioxide (CO<sub>2</sub>), water vapour and soot particles form. Soot plays a vital role in radiant energy levels. Soot that is being oxidized emits significant radiant energy, more than other combustion products. However, in very smoky flames where soot production is high it acts to block radiant energy as the soot is not being oxidised. Methanol and LNG fires have light coloured flames and hydrogen fires are invisible due to the lack of soot. Their radiant energy fraction is low compared with heavier hydrocarbons like gasoline or solvents.
- (iii) Fire plume zone:  
where the residual combustion takes place, ambient air is entrained and the temperature in the plume decreases rapidly with height.

#### **6.6.1.2 Parameters affecting pool fires**

The key parameters are:

- burning rate of flammable material
- shape of the flame
- direction or orientation of the flame
- amount of soot produced
- effect of wind drag on the flame
- carbon to hydrogen ratio
- oxygenation level of substance

### 6.6.1.3 Evaluation of heat radiation on targets

The intensity of the radiation is dependent on the rate of burning, the form of the combustion products (lots of smoke or clean flame) and the atmospheric conditions (e.g. dry or humid day). It is also clearly dependent on the distance of the receptor from the flame.

From a modelling perspective there are two basic approaches to represent the heat radiation intensity at a specified distance from the fire. These are:

- point source model
- view factor model.

The first idealises the fire as emanating from a single point, whilst the second sees the shape of the flame and the view which the receiver has of it as being important. Figure 6-9 shows the conceptual differences. Clearly the point source approach is simple and very idealised. However for distances far from the fire it provides a useful prediction. For distances close to the flame it tends to over-estimate the heat radiation. The view factor approach is more complicated since we need to calculate the "view-factor" which represents a measure of how much of the flame shape is "seen" by the receptor (the solid angle subtended on the flame within the view of the target).

In many cases the view-factor can be quite small, thus reducing the incident radiation on the receptor. This is a very important factor in obtaining credible thermal radiation impacts.

### 6.6.1.4 The point source model

The point source model depends on

- (i) The total energy release via combustion
- (ii) The fraction of total energy radiated ( $f$ )
- (iii) The amount of energy transmitted to the receptor (transmissivity)
- (iv) The distance to the target

Table 6-10 gives the point source model.

**TABLE 6-10 POINT SOURCE FIRE RADIATION MODEL**

The heat flux,  $Q$  at a distance  $x$  from the fire centre is given by:

$$Q = \frac{MH_c f \tau}{4\pi x^2} \quad (6.16)$$

where:

$Q$	= heat flux (kW/m <sup>2</sup> )
$M$	= rate of combustion (kg/s)
$H_c$	= heat of combustion (kJ/kg)
$f$	= fraction of thermal energy radiated (0.15 - 0.35)
$x$	= distance from flame centre to observer (m)
$\tau$	= atmospheric transmissivity (0.5 - 0.8)

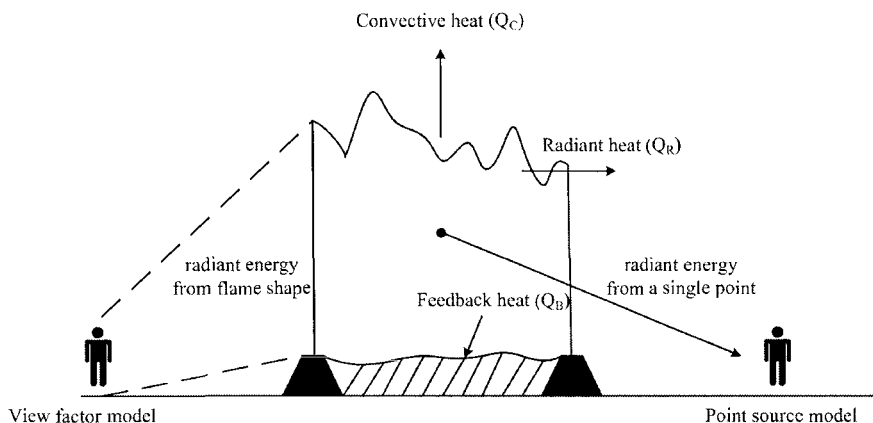


**FIGURE 6-9 POOL FIRE MODEL CONCEPTS**

The radiant fraction ( $f$ ) is that fraction of the heat of combustion which goes into radiant energy. Typical values over a range of fire diameters are:

methanol	= 0.16 - 0.18
butane	= 0.20 - 0.27
benzene	= 0.34 - 0.36
LNG	= 0.20 - 0.27
gasoline	= 0.14 - 0.30

Typically as the pool diameter increases for high sooting materials, the radiant fraction ( $f$ ) reduces. Heptane for example has a radiant fraction of 0.35 for pool sizes up to 3m, then reduces to 0.2 for pool diameters of around 10m.

The transmissivity,  $\tau$  depends strongly on the amount of moisture in the air and this is measured by relative humidity (RH). It is also a function of distance. An approximation can be used, given by

$$\tau = \log_{10} \left[ 14.1(RH)^{-0.108} r^{-0.13} \right] \quad (6.17)$$

where:

$RH$	= percent relative humidity
$r$	= distance (m)

A rough guide is also given by Table 6-11.

**TABLE 6-11 APPROXIMATE VALUES FOR TRANSMISSIVITY AT 40% RH**

$r(m)$	$\tau$
50	0.75
100	0.70
500	0.60
1000	0.58

A maximum burning rate ( $M$ ) can be estimated from the size of the pool and the burning rate per unit area ( $\dot{m}$ ) given by:

$$\dot{m} = \frac{1 \times 10^{-3} H_C}{(H_V + C_p \Delta T)} \quad (6.18)$$

where:

$$\begin{aligned} H_C &= \text{heat of combustion (kJ/kg)} \\ H_V &= \text{heat of vaporization (kJ/kg)} \\ C_p &= \text{heat capacity of the material (kJ/kgK)} \\ \Delta T &= (T_{\text{boiling}} - T_{\text{ambient}}) (\text{K}) \end{aligned}$$

Typical values of  $\dot{m}$  are around 0.05-0.10 kg/m<sup>2</sup>.s. The burning rate ( $M$ ) is then simply  $M = \dot{m} A$ , where  $A$  is the pool area (m<sup>2</sup>). This is a conservative estimate.

The flame height ( $h_f$ ) can be predicted by the Thomas correlation (Thomas 1963).

$$h_f = 42 d_p \left[ \frac{\dot{m}}{\rho_a \sqrt{g d_p}} \right]^{0.61} \quad (6.19)$$

where:

$$\begin{aligned} d_p &= \text{pool diameter (m)} \\ \rho_a &= \text{density of air (kg/m}^3\text{)} \simeq 1.2 \text{ kg/m}^3 \text{ at } 20^\circ\text{C} \\ \dot{m} &= \text{burning rate per unit area (kg/m}^2\text{.s)} \\ g &= 9.81 \text{ m/s}^2 \end{aligned}$$

#### EXAMPLE 6-7 BURNING POOL OF GASOLINE

Consider a 4m diameter pool of gasoline which radiates to an observer 10 metres away from the pool edge. What is the heat flux at the observer? Relative humidity is 50% with ambient temperature of 20°C.

For gasoline we have:

$$\begin{aligned} H_C &= 42400 \text{ kJ/kg} & T_a &= 20^\circ\text{C} = 293\text{K} \\ H_V &= 330 \text{ kJ/kg} & C_p &= 2 \text{ kJ/kgK} \\ T_b &= 415 \text{ K} & f &\simeq 0.25 \end{aligned}$$

Using (6.18) the burning rate is:

$$M = \dot{m} A = \frac{1 \times 10^{-3} (42400)}{(330 + 2(415 - 293))} \cdot (12.56 \text{ m}^2) = 0.93 \text{ kg/s}$$

The transmissivity from equation (6.17) is:

$$\tau = \log_{10}[14.1(50)^{-0.018}(12)^{-0.13}] = 0.83$$

Note: distance from pool centre = 10m from pool edge + 2m pool radius, giving 12m.

The flame height from equation (6.19) is:

$$h_f = 42(4) \left[ \frac{0.074}{1.2\sqrt{9.81(4)}} \right]^{0.61} = 10 \text{ m}$$

Distance from the flame centre to the observer is

$$\sqrt{(10+2)^2 + (5)^2} = 13 \text{ m}$$

$$Q = \frac{0.93(42400)(0.25)(0.83)}{4\pi(13)^2} = 3.9 \text{ kW/m}^2$$

■ ■ ■

### 6.6.1.5 The view factor model

The view factor model is given in Table 6-12.

■ ■ ■

**TABLE 6-12 VIEW FACTOR MODEL**

The heat flux  $Q$  for the viewpoint model is given by

$$Q = \tau EF \quad (6.20)$$

where

$Q$	= heat flux (kW/m <sup>2</sup> )
$E$	= surface emissive power of the flame (kW/m <sup>2</sup> )
$F$	= geometric view factor.
$\tau$	= transmissivity

Emissive power ( $E$ ) is the amount of radiation flux which emanates from the surface of the flame. It is often difficult to calculate because many flames burn with a lot of smoke. Hence the bright and smoky parts emit different amounts of radiation. It is also very dependent on the degree to which air can be mixed with the fuel, and the size of the fire. It is the most uncertain of all the data used in the view factor model.

For pool fires of various hydrocarbons, we can estimate the emissive power as the composite of clear flame and smoky flame emissive powers:

$$E = E_{smoke}\psi + E_{flame}(1-\psi) \quad (6.21)$$

where:

$$E_{smoke} = \text{emissive power of smoky flame } (\sim 20 \text{ kW/m}^2)$$

$$\begin{aligned}
 E_{\text{flame}} &= \text{emissive power of clear flame } (\sim 130 \text{ kW/m}^2) \\
 \psi &= \text{fraction of smoky surface in fire}
 \end{aligned}$$

Values of  $\psi$  vary significantly, typically up to 0.8 (80%) of the flame surface. Typical maximum emissive powers of clear flames are around 130 kW/m<sup>2</sup>. Average values of  $E$  are around 40 kW/m<sup>2</sup>.

Alternately, measurements on pool fires give emissive powers ( $E$ ) (TNO 1992) as seen in Table 6-13.

**TABLE 6-13 EMISSIVE POWER OF VARIOUS POOL FIRES**

Substance	Emissive Power ( $E$ : kW/m <sup>2</sup> )
aviation fuel	60-130
kerosene:	
(small pools $\leq 10\text{m}$ )	120
(large pools $> 30\text{m}$ )	10-25
methanol	70
LNG	150-220
LPG	60 - 130

If in doubt it is best to use a range of  $E$  values to assess the sensitivity of thermal radiation impact to the change in  $E$ .

Wind tilt of flames is often important, especially when the target is close to the flame. Caution is needed when applying flame tilt models. The most widely used model is of the general form (Johnson 1992; Pritchard and Binding 1992).

$$\frac{\tan \theta}{\cos \theta} = c(Fr)^a (Re)^b \quad (6.22)$$

$$\begin{array}{lll}
 \text{where} & Fr & = \text{Froude number } (u^2/gd_p) \\
 & \theta & = \text{angle of flame tilt, radians} \\
 & Re & = \text{Reynolds number } (ud_p/\nu) \\
 & \nu & = \text{kinematic viscosity of air (m}^2/\text{s)} (\sim 1.5 \times 10^{-5} \text{ @ } 20^\circ\text{C})
 \end{array}$$

Rew and Hulbert (1996), suggest that the simplest model, with the best data fit, is given by:

$$\frac{\tan \theta}{\cos \theta} = 3.13 Fr^{0.431} \quad (6.23)$$

There was virtually no dependence on  $Re$  from the data fitting.

View factors are calculated based on the geometry of the flame and the receiver. These are typically much less than 1.0. For a pool fire we can idealise the situation in two ways:

- consider the flame as a cylinder or tilted cylinder
- consider the flame as a flat surface



### Tilted cylinder view factors

Consider the flame as a tilted cylinder of radius  $r$ , flame length  $L$  and tilt of  $\theta$ . The receiver is located a distance  $x$  from the centre of the flame as shown in Figure 6-10.

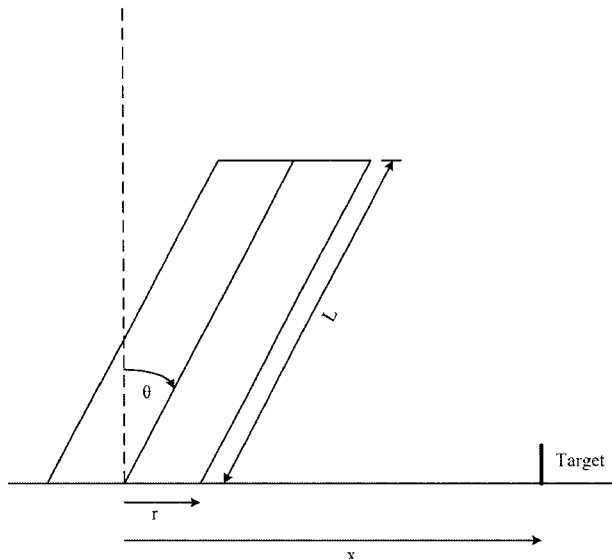


FIGURE 6-10 CYLINDRICAL FLAME VIEW FACTOR

For an event we need to estimate two key measurements

$$L_r = \frac{L}{r}; \quad x_r = \frac{x}{r} \quad (6.24)$$

The maximum view factor ( $F_{max}$ ) is the root mean square of horizontal ( $F_h$ ) and vertical ( $F_v$ ) factors.

For a vertical flame ( $\theta = 0$  radians), the maximum view factor  $F_{max}$  is given in Figure 6-11 (TNO 1997). View factor expressions for  $F_v$  and  $F_h$  are available for tilted flames (TNO 1997; Lees 2001). These are best computed from the mathematical expressions. For values of  $x_r = 10$  and  $L_r = 5$  and a tilt of  $30^\circ$ , the view factor increases by about 25%.

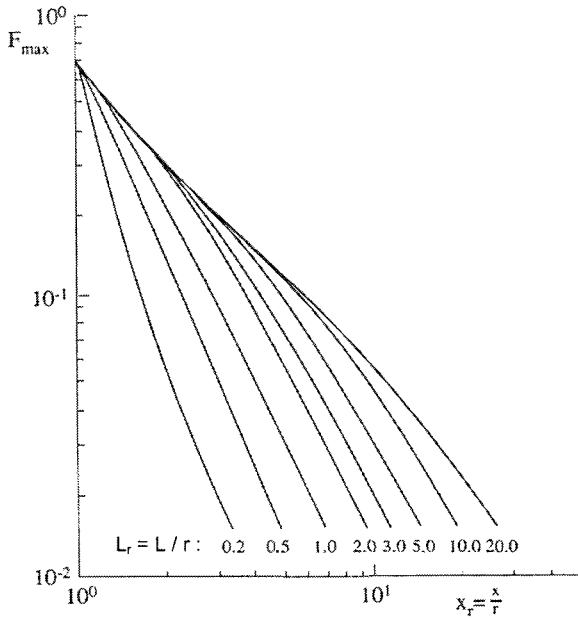


FIGURE 6-11 CYLINDRICAL FLAME MAXIMUM VIEW FACTOR ( $\theta = 0$  RADS) (TNO 1997)

### Vertical flat surface view factors

This is a useful idealisation for cases where the pool is large or confined to a rectangular, bunded area. The situation is shown in Figure 6-12 where the flame is the vertical surface of height  $L$  and length  $2b$  with receiver located centrally and at a distance  $x$ . Again it is necessary to define two dimensionless parameters,

$$L_r = \frac{L}{b}; \quad x_r = \frac{x}{b} \quad (6.25)$$

The values of the maximum view factor are shown in Figure 6-13. (TNO 1997)

If the pool is rectangular with length/width  $< 2$  then an equivalent diameter can be used, given by

$$d_p = d_{eq} = \frac{4 \times \text{pool area}}{\text{pool perimeter}} \quad (6.26)$$

and this can be used with the tilted cylinder view factor to estimate the value of  $F_{max}$ .

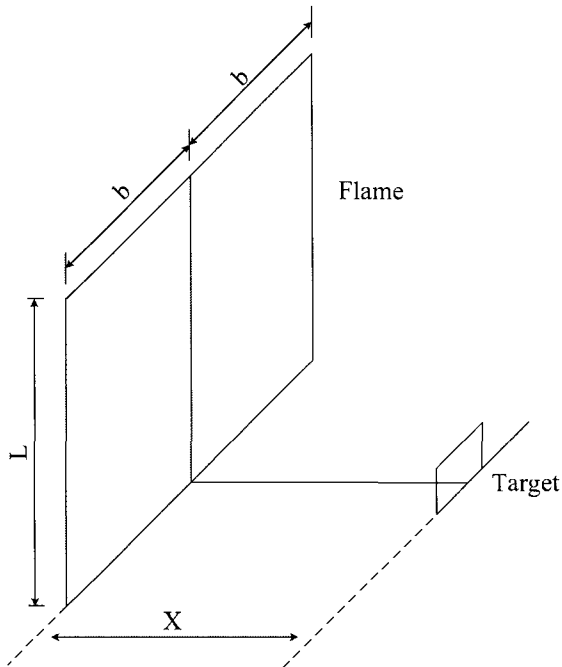


FIGURE 6-12 VERTICAL FLAME GEOMETRY VIEW FACTOR GEOMETRY

#### EXAMPLE 6-8 BURNING GASOLINE

Consider Example 6-5 of a 4m diameter pool of gasoline and an observer at 10m from the pool. Windspeed  $u = 0$  m/s.

Previously:  $\dot{m} = 0.074 \text{ kg/m}^2 \text{ s}$  and flame height = 10m

From equation 6.21, emissive power of flame is given by

$$E = 0.8(20) + 0.2(140) = 44 \text{ kW/m}^2$$

and transmissivity  $\tau = 0.83$ .

The view factor (as a cylinder) with  $L_r = \frac{10}{2} = 5$ ;  $x_r = \frac{12}{2} = 6$  gives

$$F_{\max} = 0.075 \text{ (Figure 6-11).}$$

Heat flux at target,  $Q = \tau EF = 0.83(44)(0.075) = 2.7 \text{ kW/m}^2$ .

This is smaller than that predicted by the point source method.

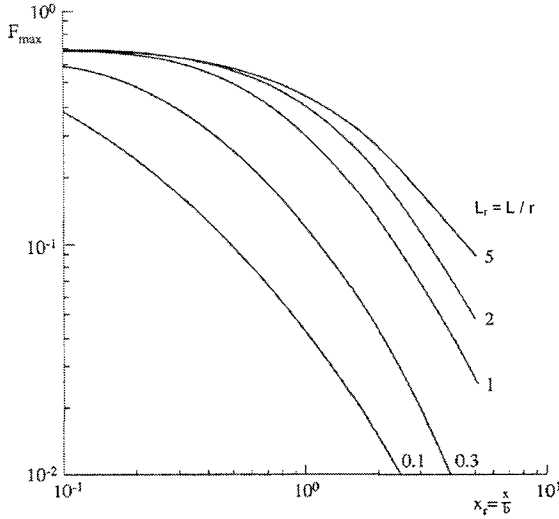


FIGURE 6-13 VERTICAL FLAME MAXIMUM VIEW FACTOR (TNO 1997)

The previous model based on the view factor method and given by equation 6.20, can be improved by considering separately the clear flame and smoky flame portions to arrive at:

$$Q = \tau E_{cf} F_{cf} + \tau E_{sf} F_{sf} \quad (6.27)$$

where:

$$\begin{aligned} E_{cf} &= \text{clear flame emissive power (kW/m}^2\text{)} \\ F_{cf} &= \text{clear flame view factor} \\ E_{sf} &= \text{smoky flame emissive power (kW/m}^2\text{)} \\ F_{sf} &= \text{smoky flame view factor} \end{aligned}$$

This is the model advocated by Rew and Hulbert (1996), based on earlier work by Pritchard and Binding (1992). It gives superior results to the more simplistic models but relies on predicting clear flame length, which is given by Pritchard and Binding (1992) as:

$$\frac{L_{cf}}{D} = 11.404 (\dot{m}_*)^{1.13} (u_9^*)^{0.179} \left( \frac{C}{H} \right)^{-2.49} \quad (6.28)$$

where:

$$\begin{aligned} \dot{m}_* &= \dot{m} / [\rho_a (g d_p)]^{\frac{1}{2}} \quad (\text{scaled burning rate}) \\ u_9^* &= u_9 / [(g \dot{m} d_p / \rho_a)]^{\frac{1}{3}} \quad (\text{scaled burning rate}) \\ \frac{C}{H} &= \text{carbon to hydrogen ratio of the burning material} \\ u_9 &= \text{windspeed at height of 9m (m/s)} \\ \rho_a &= \text{air density (kg/m}^3\text{)} \simeq 1.2 \text{ kg/m}^3 \text{ at } 20^\circ \text{C} \end{aligned}$$

### 6.6.1.6 Limitations

It should be remembered that uncertainties in radiation level predictions arise at each substep of the estimation process. The most crucial aspects are the emissive powers used in the estimate. If field data, such as LNG or LPG emissive powers are available then they should be used rather than correlations. It is important to perform sensitivity studies to check the effect of assumed values of  $E_{cf}$  and  $E_{sf}$ .

### 6.6.2 Boiling Liquid Expanding Vapour Explosions (BLEVEs)

In the case of a BLEVE, we can idealise the fire situation as a large fire ball suspended above the ground. Emissive power is usually high since fuel-air mixing is good. Typically the emissive power at the surface is in the range of 200-350 kW/m<sup>2</sup>.

Of importance is the size of the fire ball and the duration of burning. Extensive work by TNO after the PEMEX disaster in Mexico City in 1984 led to correlations for these basic parameters as shown in Table 6-14 (TNO 1985).

**TABLE 6-14 BLEVE CORRELATION MODEL**

The TNO BLEVE correlations are:

$$D = 6.48 W^{0.325} \quad (6.29)$$

$$t = 0.852 W^{0.260} \quad (6.30)$$

where:

$D$	= diameter of fireball (m)
$t$	= duration (s)
$W$	= weight of fuel (kg)
$H$	= bottom height = 0.5 $D$ (m)

The idealised situation is seen in Figure 6-14.

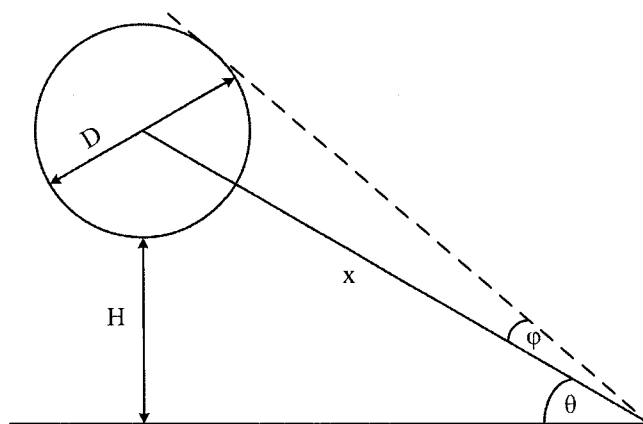


**FIGURE 6-14 IDEALISED BLEVE MODEL**

The view factor method is used to estimate the radiation intensity at the receiver. This is given by:

$$Q = \tau E F$$

with

$$\begin{aligned} Q &= \text{received flux (kW/m}^2\text{)} \\ F &= \text{view factor} = D^2 \cos \theta / 4x^2 \quad (\theta \leq 90^\circ - \phi) \\ E &= \text{emitted flux} \cong \varepsilon \sigma T_s^4 \end{aligned}$$

where

$$\begin{aligned} \varepsilon &= \text{emissivity } (\sim 1.0) \\ \sigma &= \text{Stefan-Boltzmann constant} = 5.67 \times 10^{-11} \frac{\text{kW}}{\text{m}^2 \text{K}^4} \\ T_s &= \text{flame surface temperature (K)} \\ \tau &= \text{transmissivity} \end{aligned}$$

The above view factor is applicable when the fire ball is in full sight of the receiver. In cases where  $\theta > 90^\circ - \phi$  not all of the fireball is seen by the receiver and the view factor becomes more complex. (see TNO 1997; Lees 2001).

#### EXAMPLE 6-9 BLEVE INCIDENT

A storage tank releases 20,000 kg of LPG which ignites and forms a fireball. What is the radiation intensity 200m from the incident?

TNO correlations give (6.29) and (6.30):

$$\begin{aligned} D &= 6.48 (20,000)^{0.325} = 162 \text{ metres} \\ t &= 0.852 (20,000)^{0.260} = 11 \text{ seconds} \end{aligned}$$

Heat flux at 200m from fireball centre

$$\text{If } E = 250 \text{ kW/m}^2 \text{ with the view factor at maximum } (\theta = 0^\circ)$$

$$Q = \tau E F \cong 0.7(250) \frac{D^2}{4x^2} = 0.7(250) \frac{(162)^2}{4(200)^2} = 29 \text{ kW/m}^2$$

At this radiation level there would be significant injuries and some fatalities for exposure over the duration of the fireball.

### 6.6.3 Jet Fires and Spray Fires

Here we are concerned about fires which result from the ignition of a high velocity jet of gas and/or liquid escaping from a pipe or vessel.

This type of fire can occur when there are discharges from safety valves such as in the case of LPG storage or from holes in pipes, or vessel walls, or gasket leaks

### 6.6.3.1 Characteristics of jet fires

Jet fires are high momentum releases of burning hydrocarbon or combustible substances, either in liquid or gaseous form. Their burning characteristics depend strongly on the flammable material, the release pressure and the state of the substance. For release of liquefied gases, there is the phenomenon of flashing and droplet formation that affects the subsequent fire. Jet fires burn with considerably more emissive power than pool fires. The flames are affected by buoyancy such that horizontally released jets often have significant “turn up” along the jet fire due to buoyancy of the hot combustion gases. Wind can also have significant impacts in cooling and shortening vertical and angled jet fires.

For high velocity jets, there is often a significant “lift off” distance where a region of no flame is seen near the release point. Here the liquid or gas is rapidly expanding, mixing with air and travelling at very high velocity such that the flame cannot burn back to the discharge point. These characteristics have been well documented and in some cases captured in current models (Chamberlain 1987; Johnson et al. 1994; Crowley et al. 1992).

A particularly difficult situation is dealing with the directionality of the jet fire, especially where ground or nearby vessel impingement changes the “natural” flame shape. Here, specialized models are needed based on computational fluid dynamics (Johnson et al. 1999).

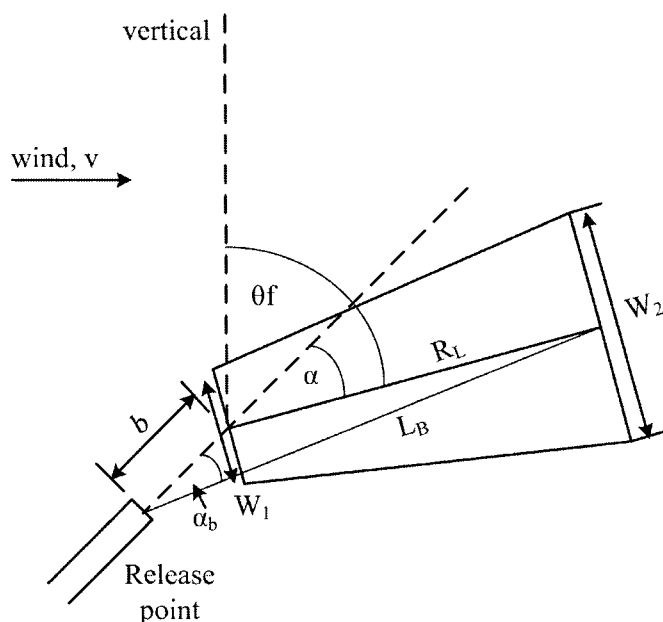


FIGURE 6-15 JET FIRE IDEALISATION (Chamberlain 1987)

### 6.6.3.2 Models for jet fires

Simplistic approaches to jet fire modelling have existed in a number of engineering standards (API RP521, 1997). These represent flares as a single point source radiating to a target. Modified approaches that divide the flame into multiple point source segments are also used. These approaches can be useful for initial, rough estimates.

The most widely used jet fire model is that developed by Chamberlain (1987), commonly known as the “Thornton” model due to the work of Shell Research Ltd at their Thornton facility. Further developments by Johnson et al. (1994) addressed the issue of horizontally oriented jet fires. The conceptualization of the fire as the frustum of a cone is seen in Figure 6-15. Here the jet fire has a discharge angle of  $(\theta_f - \alpha)$  from the vertical with a flame tilt due to wind of  $\alpha$ . The flame lift off is given by the distance,  $b$ . The flame length ( $L_b$ ), base and tip dimensions of the cone frustum ( $W_1$ ,  $W_2$ ) are given by correlations (Chamberlain 1987).

Once these key dimensions are estimated it is then possible to consider thermal radiation impacts on targets in the vicinity of the jet fire. These estimates are based on the view factor method as given in equation (6.20). The surface emissive power ( $E$ ) can be estimated as:

$$E = \frac{F_s Q}{A} \quad (6.31)$$

where:	$F_s$	= fraction of heat radiated = $0.21e^{-0.00323u_j} + 0.11$
	$u_j$	= gas velocity at the exit (m/s)
	$Q$	= net combustion energy (kW)
	$A$	= surface area of the frustum (m <sup>2</sup> )

Values of  $F_s$  are in the range of 0.15 to 0.30. The view factor can be obtained by assuming an equivalent tilted cylinder geometry (TNO 1997) or by integration of the standard view factor formula (Holman 1981).

Simple semi-empirical models, based on experiments with vertical flares were developed by Cook et al. (1987). These correlations, as well as the Chamberlain model (1987) are applicable for vertical and angle flames, where wind momentum dominates over buoyancy. These are not suitable for horizontal jet fires. An extension of the Chamberlain model was developed by Johnson et al. (1994) from tests with horizontal jet flames. It includes the effect of buoyancy lifting the flame above the horizontal, and the effect of wind momentum.

#### EXAMPLE 6-10 NATURAL GAS JET FIRE IMPACTS

Figure 6-16 shows the thermal radiation levels for a 10 MPa natural gas jet fire released at 5° from the vertical, subject to windspeeds of 0, 5 and 10 m/s. The gas release rate is 25.0 kg/s. The release height was at ground level and the target is downwind of the release point (Daesim 2004). The model is based on the work of Chamberlain (1987).

It can be seen that in the far field ( $> 60$  m) the incident radiation is essentially the same for all windspeeds. However, in the near field, there are substantial





differences in thermal radiation levels due to the flame tilt and shortening under different windspeeds.

### 6.6.3.3 Limitations

The current models for jet fires provide good, validated approaches to fire radiation estimates that are based on a wide range of field experiments. The most significant limitation of these models is when impingement of the flame occurs. In these cases special approaches are required that use computational fluid dynamics (CFD) methods (Johnson et al. 1999).

Also nearly all the field work on jet fires has used natural gas or propane. When other substances are involved it is important that a range of emissive powers are investigated to check the predicted range of radiation levels on the target.

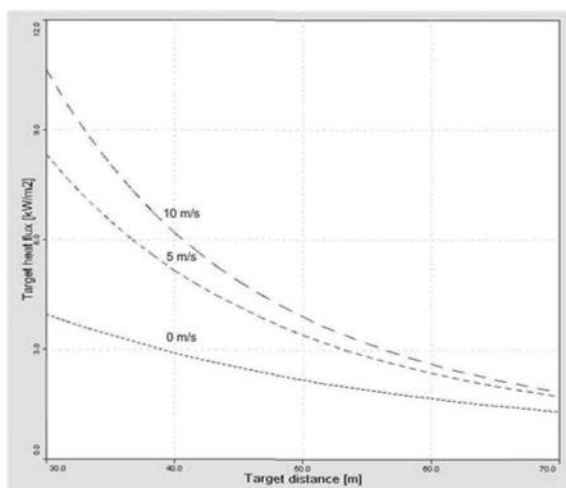


FIGURE 6-16 METHANE JET FIRE THERMAL RADIATION IMPACTS (DAESIM 2004)

## 6.7 EFFECTS MODELLING OF EXPLOSIONS

### 6.7.1 Characteristics of Gas Explosions

Explosions are one of the most devastating events which occur in the process industries and also in transport situations. In most cases we are dealing with flammable vapour-air mixtures or solid-air mixtures which are ignited in some way by flame, friction, sparks or heated surfaces. These mixtures could be hydrocarbons like LPG (propane or butane) or dusts such as sugar or coal (Guilbert and Jones 1996). In many cases very little energy is needed to initiate the combustion processes which lead to the explosive event.

The types of structural damage effects resulting from a range of explosion overpressures are given in Chapter 7, Table 7-4. In mining applications dense phase explosions often need to be addressed.

These effects are the result of the enormous amounts of energy released over a short period of time when the explosion occurs. The important factors and principal approaches to predicting these events are given in Table 6-15.

**TABLE 6-15 EXPLOSION CHARACTERISTICS AND PREDICTION METHODS**

Important Factors	Methods of Prediction
<ul style="list-style-type: none"> <li>• Peak overpressure</li> <li>• Positive phase duration</li> <li>• Degree of confinement</li> <li>• Pressure impulse</li> </ul>	<ul style="list-style-type: none"> <li>• TNT Equivalent models</li> <li>• TNO Multi-Energy model</li> <li>• 3D Mechanistic models</li> </ul>

Explosions in process systems can be related to a number of events which include:

- (i) The escape of flammable liquid or gas that subsequently forms a combustible fuel-air mixture and is subsequently ignited. In this case there is a vapour cloud explosion of varying effects depending on the degree of confinement of the explosive mixture.
- (ii) The ignition of a flammable mixture in the vapour space of storage tanks. The ignition can be due to static electricity, direct flame or sparks from maintenance operations. In this case, roof design and venting should relief pressures but explosions can result in major structural damage.
- (iii) The ignition of flammable materials in process vessels due to autoignition or other direct causes such as static discharges or explosive reactions that can propagate through adjoining pipework or lead to vessel disintegration. Blast waves and blast fragments are major results of such incidents.
- (iv) The ignition of fine particulates such as coal dust, sulphur, aluminium and combustible grains that can lead to devastating explosions that destroy storage and handling facilities as well as generate significant blast waves and fragments.

#### EXAMPLE 6-11 EXPLOSION INCIDENTS

- a) A 15,000 m<sup>3</sup> ethanol storage tank was destroyed in January 2004, at a storage facility in NSW, Australia when the vapour space was ignited during maintenance work on the tank. The roof was blown onto the foam generation station and a nearby tanker loadout facility and the subsequent fire burned for many hours before being extinguished.
- b) The release of large amounts of cyclohexane in the Nypro works at Flixborough in 1974 lead to a massive vapour cloud explosion that destroyed the control room killing 28 personnel. It caused significant damage at the nearby village. The explosion varied in its intensity due to significant areas of confinement within the cloud.

In relating the key explosion factors to ultimate damage we need to know both values of peak overpressure  $p_o$  and the positive phase duration  $t_p$ . In Section 7.3 an approach based on probit functions utilising information on pressure-time profiles

provides estimates of impacts on people and structures. Figure 6-17 shows typical incidents related to vapour cloud explosions.

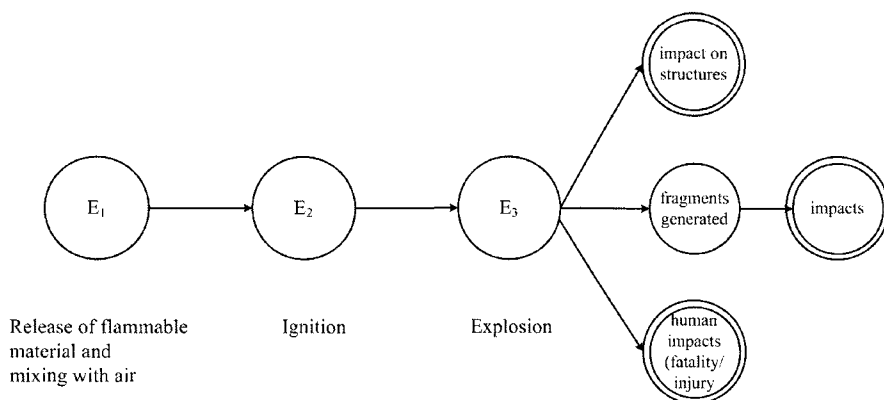


FIGURE 6-17 TYPICAL VAPOUR CLOUD EXPLOSION INCIDENT

### 6.7.2 Explosion Overpressure and Phase Duration

It was recognised since the time of the Flixborough incident that a facility design should include limiting explosion damage (Lawrence and Johnson 1974). It can be seen from Table 6-15 there are 4 key factors in an explosion. These are related to the overpressure which is the pressure rise above normal atmospheric pressure, the positive phase duration which is the time during which the pressure is above atmospheric pressure, the degree of confinement of the flammable mixture which causes acceleration of the flame front and influences the overpressure, and the impulse (area under the pressure-time profile).

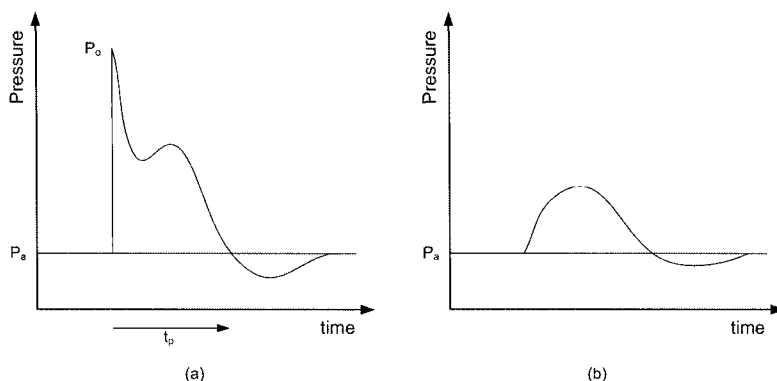


FIGURE 6-18 PRESSURE CHANGE PATTERNS FROM EXPLOSION EVENTS

Figure 6-18 shows two typical pressure change patterns which could be experienced from an explosion event. The first shows a step increase in pressure from atmospheric pressure  $p_a$  to  $(p_a + p_o)$ , followed by a sharp drop in pressure over

a period  $t_p$ , which is the positive phase duration (typically milliseconds). The pressure then reaches atmospheric pressure again and proceeds below atmospheric pressure during the negative phase duration, finally settling back to normal pressure as the shock wave passes by. This sharp rise in pressure in Figure 6-18(a) is typical of detonations where the propagation speed is anywhere between 2 and 10 km/s. Condensed explosives (e.g. TNT, PETN, RDX, C4) behave like this. For example, C4 plastic explosive has a detonation velocity of around 8.1 km/s. The maximum overpressures ( $p_o$ ) can be as high as 15-18 bar (1500-1800 kPa). The second peak in Figure 6-18(a) is associated with the reflected pressure wave from the ground.

In the second case seen in Figure 6-18(b), the blast wave rises more gradually to the peak overpressure and then gradually subsides. The positive phase duration is longer than the shock wave but the overpressure is greatly reduced. Typically, these slower burning combustion processes have overpressures in the range 0.05 - 0.7 bar (5 - 70 kPa) and  $t_p$  values around 0.3 - 1.5 seconds for process plant incidents. In offshore oil and gas facilities with plated decks, the flammable cloud is confined between the floor and roof of a deck. This confinement, together with the congestion of equipment on board can cause overpressures up to 2-3 bar or higher.

The last key factor is the degree of confinement. This is a very difficult factor to assess in practice as it has a significant and direct influence on the peak overpressure. The degree of confinement directly affects the combustion processes by improving mixing or turbulence of the burning flame front and thus helps accelerate the propagation of the pressure wave. This confinement and hence acceleration can help explain the dramatic change in patterns of blast damage seen in open areas versus confined areas. Here the explosion assumes the characteristics of a detonation with a significant increase in blast wave velocity. The degree of confinement directly affects the 'blast strength' often used in the TNO Multi-Energy model as discussed in Section 6.7.3.2. Any use of this factor needs to be accompanied by sensitivity analyses to assess its importance.

In the following sections we look at several approaches to predicting the physical effects resulting from explosions.

### 6.7.3 Methods of Estimating Explosion Impact

In the following three sections we discuss the principal models used for explosion predictions. These are the TNT equivalent model, the TNO multi-energy model (MEM) and use of computational fluid dynamics (CFD) models. Other models exist but in many cases have been superseded by the models discussed here.

#### 6.7.3.1 TNT equivalent models

TNT equivalent models attempt to convert the amount of flammable material in the vapour cloud into an equivalent amount of TNT. Much is known about the blast effects of TNT through military and industrial use, hence the motivation to use well established data.

The procedure is relatively simple and the major steps in applying this method are:

- Estimate the size of the flammable fuel cloud
- Convert the fuel mass to a TNT equivalent
- Convert the target distance to a "scaled" distance
- Determine the overpressure from TNT correlations.

However, it must be borne in mind that there are some limitations to the method. These include:

- Under-predicts overpressure for partial confinement
- TNT-blast decays faster than VCE blast
- Gas explosions are variable in strength
- Efficiency of explosion is highly empirical
- Assumes detonation explosion
- TNT explosion is mechanistically different to VCE.

In particular the efficiency of the explosion, which is the fraction of total energy converted to blast energy, is highly variable.

**TABLE 6-16 THE TNT EQUIVALENT MODEL**

The TNT equivalent (kg) is given by:

$$W_{TNT} = \alpha \cdot \frac{W \cdot H_c}{H_{TNT}} \quad (6.32)$$

where:

$W$	= weight of fuel in the cloud (kg)
$H_c$	= heat of combustion of the fuel (kJ/kg)
$H_{TNT}$	= TNT blast energy (5420 kJ/kg)
$\alpha$	= explosion efficiency.

The explosion efficiency ( $\alpha$ ) has considerable variability. Typically  $\alpha = 0.04$  for hydrocarbons;  $\alpha = 0.10$  for highly reactive substances. Some practitioners suggest that three classes can be used, based on reactivity:

Class I:	$\alpha = 0.05$ (propane, butane, flammable liquids)
Class II:	$\alpha = 0.10$ (ethylene, ethers)
Class III:	$\alpha = 0.15$ (acetylene)

Once the TNT equivalent is known the overpressure values are predicted using a "scaled" distance, based on the actual distance from the blast and the TNT equivalent. This scaled distance  $z$  is given by:

$$z = \frac{R}{(W_{TNT})^{\frac{1}{3}}} \quad (6.33)$$

where:  $R$  = distance from blast (m)  
 $W_{TNT}$  = kg equivalent of TNT (kg)

From extensive military testing of TNT in the USA and UK, field data has led to the representation of scaled parameter plots for overpressure, arrival and positive phase duration times as well as impulse. Figure 6-19 shows the scaled parameters against scaled distance as given in equation 6.30 (Lees 2001). These parameters are for a ground level blast where reflection is an additional contributor to the total overpressure.

The scaled parameters are defined as:

$$\text{Scaled overpressure:} \quad P_s = P_o / P_a \quad (6.34)$$

$$\text{Scaled positive phase duration:} \quad \tau_d = \frac{t_p}{W^{\frac{1}{3}}} \quad (6.35)$$

$$\text{Scaled arrival time:} \quad \tau_a = \frac{t_a}{W^{\frac{1}{3}}} \quad (6.36)$$

$$\text{Scaled impulse:} \quad i_s = \frac{i_p}{W^{\frac{1}{3}}} \quad (6.37)$$

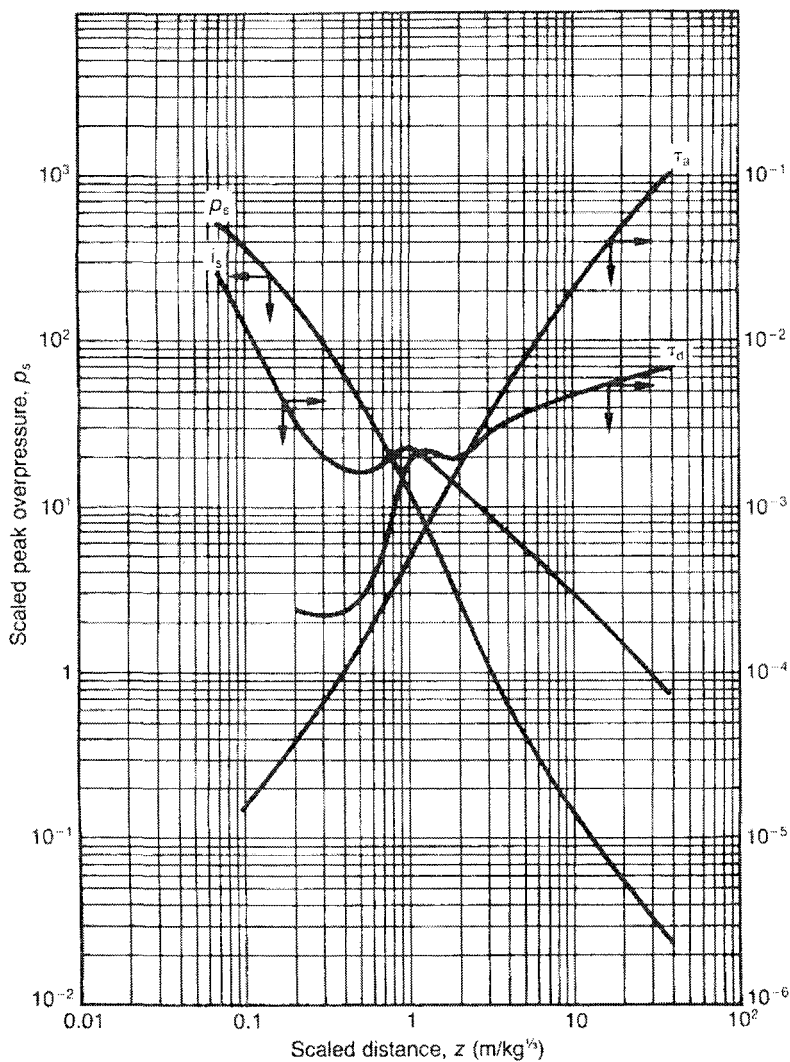


**FIGURE 6-19 SCALED PARAMETER PLOTS FOR TNT EXPLOSIONS (Lees 2001)**

For ease of computation, the scaled distance and peak overpressure are expressed in the following correlation, based on the curves developed by Brasie and Simpson (1968).

$$\log_{10}(10 \cdot z) = 0.082 (\log_{10} p_o)^2 - 0.529 \log_{10} p_o + 1.526 \quad (6.38)$$

Where  $p_o$  is the explosion peak overpressure in bars. Equation (6.38) is valid for  $p_o$  falling in the range 0.01 to 1 bar.

**EXAMPLE 6-12 EXPLOSION OF PROPYLENE**

A propylene liquid storage tank of 25,000 kg capacity (at 20°C) suffers a major failure with the loss of propylene. Using the TNT equivalent method the overpressures can be estimated.

Relevant data includes:

$$\begin{aligned}\Delta H_v &= 438 \text{ kJ/kg} \\ C_p &= 2.6 \text{ kJ/kgK} \\ H_c &= 46,400 \text{ kJ/kg} \\ \text{Normal boiling point} &= -47.8^\circ\text{C} = 226 \text{ K}\end{aligned}$$

The flash fraction from equation (6.7) gives

$$\phi = 1 - \exp \left[ - \frac{2.6}{438} (293 - 226) \right] = 0.33$$

The entrained fraction is  $e = 0.33$ , and cloud mass =  $(e + \phi)W_o = 16,500 \text{ kg}$ .

Equivalent weight of TNT is given by equation (6.32)

$$W_{TNT} = \alpha \cdot \frac{W \cdot H_c}{H_{TNT}} = \frac{0.1 (16,500) 46,200}{5420} = \underline{14,000 \text{ kg}}$$

The following table of distances, scaled values and overpressures can be then generated.

Distance R(m)	Scaled distance Z	Overpressure (kPa)
50	2.1	160
100	4.2	39
200	8.3	13
500	20.1	4
1000	41.5	1.8
2000	83.0	8

■ ■ ■

It is estimated that severe structural damage will be experienced out to 100m and 90% window breakage to 500m.

**6.7.3.2 Multi-Energy Model**

The Netherlands Organization for Applied Scientific Research (TNO) has conducted extensive research into blast models (van den Berg 1985; van den Berg et al. 1991; Mercx et al. 1998, 2000). The TNO multi-energy model allows for blast strength to be incorporated. Using this technique it is possible to adjust predictions to account for partial confinement of the vapour cloud. The method considers the total cloud as a series of sub-explosions corresponding to the various confined or unconfined regions. The confined regions might be parts of the cloud located under tanks or vessels, hemmed in by buildings or other structures. Similar



results are obtained from flame speed based models such as the Baker-Strehlow method (Baker et al. 1996; Tang and Baker 2000).

In comparison with TNT equivalent models of vapour cloud explosions where blast effects decay quicker than reality, the multi-energy model can help predict far field effects more accurately.

The key additional factor in this model is the 'blast strength' which ranges from 1 (insignificant) to 10 (detonative strength). Figures 6-20 and 6-21 show the overpressure and positive phase duration versus an energy scaled distance. Separate curves relate to the blast strength. The model is shown in Table 6-17.

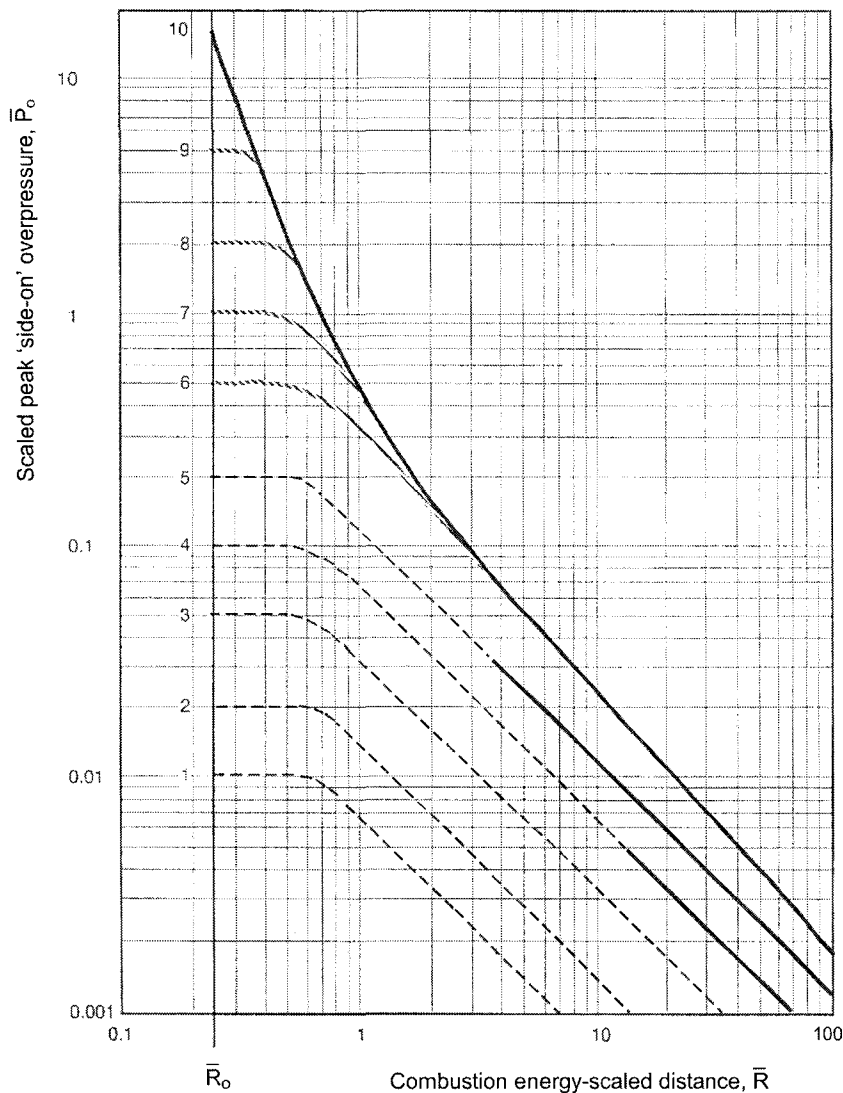


FIGURE 6-20 SCALED PEAK SIDE OVERPRESSURE FOR MEM (BY PERMISSION OF ELSEVIER)

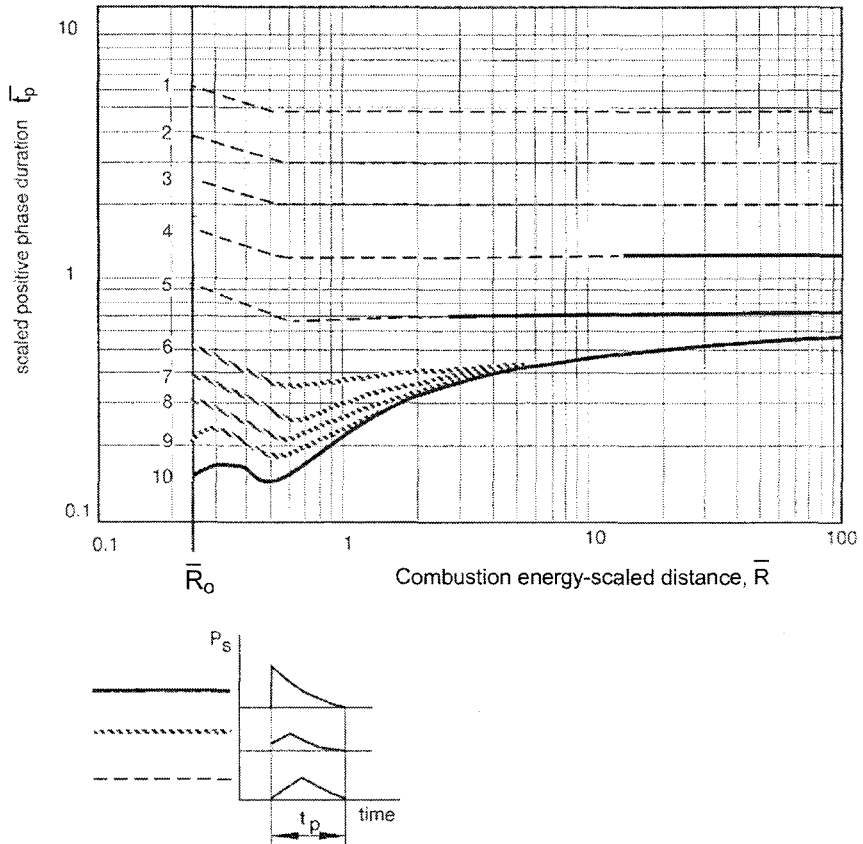


FIGURE 6-21 SCALED POSITIVE PHASE DURATION FOR MEM (BY PERMISSION OF ELSEVIER)

To apply this method the following steps need to be carried out.

- Assign portions of the cloud to different areas (e.g. between buildings, under vessels, in open air)
- Determine the fuel present in each zone (i.e. amount of gas-air mixture ( $\text{m}^3$ )) and total cloud energy,  $E$  ( $\equiv V_o E_c$ ), based on the heat of combustion of the fuel. A typical energy density  $E$  is  $3.5 \times 10^6 \text{ J/m}^3$ .
- Assign initial strengths to these vapour cloud charges (e.g. 2 for open area, 5-6 confined, 7-10 highly confined).
- Calculate scaled distances for each charge at nominated distances,  $R$ .
- From figures for  $\bar{P}_o$  and  $\bar{t}_p$  versus  $\bar{R}$ , estimate overpressure and positive phase durations for each charge. If blast zones are located close to each other and the ignition is essentially simultaneous, then overpressures can be superimposed at target distances.

TABLE 6-17 THE MULTI-ENERGY MODEL (MEM)

The following parameters describe the multi-energy model (MEM):

$$\text{Scaled overpressure:} \quad \bar{P}_o = \frac{P_o - P_a}{P_a} \quad (6.39)$$

$$\text{Scaled positive phase duration:} \quad \bar{t}_p = t_p c_a \left( \frac{P_a}{E} \right)^{\frac{1}{3}} \quad (6.40)$$

$$\text{Scaled distance:} \quad \bar{R} = R \left( \frac{P_a}{E} \right)^{\frac{1}{3}} \quad (6.41)$$

where:

$P_o$	= side-on absolute blast overpressure (Pa)	$R$	= fuel-air charge radius (m)
$\bar{P}_o$	= scaled blast overpressure (-)	$\bar{R}$	= scaled distance (-)
$P_a$	= ambient pressure (Pa)	$\bar{t}_p$	= scaled positive phase duration (-)
$c_a$	= ambient velocity of sound (m/s)	$t_p$	= positive phase duration (s)
$E$	= combustion energy in fuel-air mixture (J)		

The biggest challenge in the use of the multi energy method is the selection of the charge strength. This depends on a number of factors that include:

- (i) the level of obstruction within the gas cloud.
- (ii) the ignition strength, 'high' representing a vented explosion with 'low' being a spark or flame.
- (iii) the level of confinement being either an unconfined volume or confined between surfaces.

A decision table can be constructed (TNO 1997) that considers all factors and relates these to the blast strength.

Mercx et al. (2000) attempted to provide a correlation for the charge strength  $P_o$  based on 3 key factors:

- (i) The volume blockage ratio (VBR) representing the proportion of the total volume occupied by obstacles,
- (ii) The flame length,  $L_f$  (m) representing the longest distance from the point of ignition to an outer edge of the obstacle configuration, and,
- (iii) The average obstacle size  $D$  (m).

The correlation also considered the scale of the situation and the fuel type by using the laminar burning velocity  $S_L$  (m/s) and a scale factor  $D$  (m). The correlation is

$$P_{CS} = a \left[ \frac{(VBR)(L_f)}{D} \right]^b S_L^{2.7} D^{0.7} \quad (6.42)$$

Two correlations were developed from equation (6.42). For 3D, open regions (no confinement):

$$P_{CS} = 0.84 \left( \frac{VBR.L_f}{D} \right)^{2.75} S_L^{2.7} D^{0.7} \quad (6.43)$$

and for 2D, confined cases:

$$P_{CS} = 3.38 \left( \frac{VBR.L_f}{D} \right)^{2.25} S_L^{2.7} D^{0.7} \quad (6.44)$$

Typically  $S_L$  is 0.45 m/s (methane) and 3.5 m/s (hydrogen).

These were used to predict overpressures and were found to vary by a factor of 2 compared with CFD methods.

For offshore oil and gas facilities, Kinsella (1992) has suggested an approach for selecting the charge strength, accounting for three factors:

- Congestion: If congestion is more than the threshold of 30%, it is considered 'high'.
- Strength of ignition source: Low (spark, hot surfaces), high (naked flames, welding)
- Parallel Confinement: Low for grated decks, high for plated decks.

#### EXAMPLE 6-13 PROPYLENE EXPLOSION

Consider the explosion incident in Example 6-12 but in this case 25% of the vapour cloud is highly confined whilst the rest is unconfined. The total amount was 14,000 kg or 190,820 m<sup>3</sup> of gas-air mixture. There are 2 zones to consider.

Zone 1 (confined):

$$V_o^1 = 0.25(190820) = 47705 m^3$$

$$E^{(1)} = V_o^1 . E_c = 47705(3.5 \times 10^6) = 1.67 \times 10^{11} J$$

Zone 2 (unconfined):

$$V_o^2 = 0.75(190820) = 143115 m^3$$

$$E^{(2)} = V_o^2 . E_c = 143115(3.5 \times 10^6) = 5.0 \times 10^{11} J$$

Consider the two distances of 200 and 1000 metres.

Zone 1 scaled distances are:

$$\bar{R}_{100}^1 = 200 \left( \frac{1 \times 10^5}{E^{(1)}} \right)^{\frac{1}{3}} = 1.68$$

$$\bar{R}_{1000}^1 = 1000 \left( \frac{1 \times 10^5}{E^{(1)}} \right)^{\frac{1}{3}} = 8.4$$

Zone 2 scaled distances are:

$$\bar{R}_{100}^2 = 200 \left( \frac{1 \times 10^5}{E^{(2)}} \right)^{\frac{1}{3}} = 1.17$$

$$\bar{R}_{1000}^2 = 1000 \left( \frac{1 \times 10^5}{E^{(2)}} \right)^{\frac{1}{3}} = 5.85$$

Using Figure 6-20, the scaled results for zone 1 (blast strength = 8) and zone 2 (blast strength = 2) can be estimated. Figure 6-21 gives the scaled positive phase duration.

At R = 200 metres

Zone	$\bar{R}$	Strength	$\bar{P}_o$	$P_o$ (kPa)	$\bar{t}_p$	$t_p(s)$
1	1.68	8	0.23	23.0	0.33	0.11
2	1.17	2	0.012	1.2	3.0	1.54

At R = 1000 metres

Zone	$\bar{R}$	Strength	$\bar{P}_o$	$P_o$ (kPa)	$\bar{t}_p$	$t_p(s)$
1	8.4	8	0.029	2.9	0.47	0.11
2	5.85	2	0.00232	0.23	3.0	1.54

This shows the contribution made at the respective distances by the zones of the vapour cloud using the different blast strengths and cloud quantities. The confined part of the cloud generates greater far field overpressures compared with the TNT equivalent model.



### 6.7.3.3 Models based on computational fluid dynamics

A number of gas explosion experiments with structures simulating modules of offshore oil and gas platforms were conducted by Christian Michelsen Research in Norway (Bjerketvedt et al. 1997). It was found that the measured overpressures were significantly higher than those predicted by available simple models. The need for a more fundamental approach was established.

The growing interest in the use of more fundamental approaches to explosions based on Computational Fluid Dynamics (CFD) has led to the development of a number of models, now routinely used for off-shore explosion assessments and situations with complex geometries. The MERGE project in Europe during the early 1990s sought to understand factors that would lead to improvements in CFD code predictions (Popat et al. 1996). Typical of the CFD codes are:

- (i) AutoReaGas (TNO and Century Dynamics)
- (ii) EXSIM (Exsim, Norway)
- (iii) FLACS (GexCon, Christian Michelsen Research, Norway)
- (iv) COBRA (Mantis Numerics, Advantica Technologies, UK)
- (v) CFX-4 (AEA Technology, UK)

These models are modified CFD codes with particular submodels that deal with such issues as:

- (i) Ignition and laminar flame propagation
- (ii) Turbulent flame propagation
- (iii) Combustion

The current status of CFD explosion modelling is given by Bull (2004) and Lea and Ledin (2002) who cover many issues related to the modelling, solution and validation of these codes. Of particular significance to CFD approaches are the following issues:

- (i) Use of crude approximations to complex geometries
- (ii) Considerable uncertainty in combustion sub-models
- (iii) Importance of considering pre-existing turbulence, such as high pressure gas releases
- (iv) Simple treatments of turbulence
- (v) The need for more large-scale experimentation
- (vi) The use of adaptive grid refinement and improved numerical solution schemes
- (vii) Incorporation of flame distortion phenomena and flame interactions
- (viii) Incorporating the interaction of blast-structure effects such that the movement of structures is considered on the propagation of the blast wave.

Despite the many challenges in developing and applying CFD explosion models, predictions from these codes in complex off-shore and on-shore process geometries appear to lie within a factor of 2 of the experimental data (Bull 2004). The use of such tools is a specialist area which is finding a growing acceptance and application base.

#### **6.7.3.4 Assumptions and limitations**

The TNT equivalent model can obviously be used in situations where dense phase explosions are relevant and geometries are simple. The use of TNT equivalent models for hydrocarbon-air mixtures is not recommended. However, for hydrogen-

rich gases, Hawksley (1986) has recommended the use of TNT equivalent model with a 10% explosion efficiency, based on empirical data gathered from actual explosion events.

Where the TNT equivalent model is not applicable, the multi-energy model (MEM) or the use of CFD codes is preferred. Evenso, there are still significant uncertainties in these approaches.

In the case of the MEM there are two key characteristics to be estimated. These are:

- (i) The size of the vapour cloud charge,  $E$  and
- (ii)  $P_{CS}$ , representing the maximum explosion overpressure for values of  $\bar{R}$  less than  $\bar{R}_o$ . This allows selection of the appropriate charge strength (1 to 10).

The vapour cloud charge is easy to estimate, however, the continuing problem is the estimation of charge strength. The charge strength still remains an issue of major uncertainty despite attempts to correlate it with explosion tests.

In the case of CFD codes, there is still much to be done to improve the fidelity of the predictions in complex process situations (Bull 2004; Lea and Ledin 2002). There still exists significant issues to address in the CFD sub-models that deal with combustion processes, reaction kinetics, turbulence models and grid refinement to capture length scales of the problem at sensible computation times. For situations where there are complex geometries such as off-shore processing platforms, CFD tools provide more credible predictions than TNT and MEM methods. CFD codes require significant computation times for large-scale 3D applications and are not to be considered a tool for the amateur.

Another limitation in the application of CFD models for blast analysis in offshore oil and gas facilities is that the volume of module filled by flammable gas cloud is unknown, and hence a sensitivity analysis would be required, using various module fill fractions. Assumption of full module fill may give high blast overpressures and drag, introducing over-conservatism in structural design.

## 6.8 EFFECTS MODELLING OF DISPERSION

The release of a gas or vapour and its subsequent dispersion in the atmosphere is a significant event. Many instances occur of regulated releases such as those from power stations or boilers burning natural gas, oil or coal.

Other incidents involve accidental releases due to equipment or operational failures, e.g. the release of a toxic gas such as chlorine or ammonia from storage cylinders or vessels.

In these circumstances we are interested in the downwind concentration levels which might affect workers or local communities. It gives information on exposure levels and leads to data useful for emergency response procedures.

### 6.8.1 Types of Releases

Before dealing with predictive methods for downwind gas concentrations it is important to discuss the mode of release and the behaviour of the gas. The latter

aspect is very dependent on the chemical nature of the substance (density relative to air, reactivity with atmospheric humidity) and the conditions (temperature and pressure) under which it is contained.

The first issue is the mode of release. This can be categorized as:

- Transient release
- continuous release

In the first case, there is a transient short duration release, or a momentary release of gas or "puff" which then subsequently disperses. This could occur when a safety device relieves the pressure in a system and then resets. In this case the puff of gas disperses influenced by the atmospheric conditions at the time (e.g. windspeed and stability of atmosphere).

In the second case, the release is continuous. This could be from a broken pipe, a split in a vessel or an emission from a stack. If the release varies slowly with time then we can consider it to be continuous. Where the release time is significantly shorter than the time to disperse to the distance of interest, then a transient model can be more appropriate.

The second major issue is to do with the density of the released gas in relation to that of the surrounding air. Anyone who has handled "dry ice" will know that the cold carbon dioxide ( $\text{CO}_2$ ) spreads along the ground before it heats up and gradually disperses. This leads to three basic types of dispersion:

- positive buoyant dispersion
- neutrally buoyant dispersion
- dense gas dispersion

The first type occurs when the gas has a density lower than air. This can be due to the gas temperature or the molecular weight of the gas which is lower than air, e.g. hydrogen releases. The second type of dispersion occurs when the gas has a density similar to air. The third type behaves quite differently, with initial rolling along the ground until it gains heat by entraining air and disperses as a neutrally buoyant gas. This can be the case with gases like chlorine, ammonia or refrigerated hydrocarbons.

The result of these release types is that specific models are needed for each gas release. In some cases a number of models must be used in sequence (e.g. dense gas model to neutrally buoyant model) and assessment made as to when the transition occurs.

### 6.8.2 Characteristics and Key Factors in Gas Dispersion

The dispersion of gases in the atmosphere is a complex issue affected by many parameters. Table 6-18 sets out some of the principal parameters which ultimately affect the impact of these incidents.



TABLE 6-18 CHARACTERISTICS OF GAS DISPERSIONS

TYPES OF RELEASES	ATMOSPHERIC and IMPACT
<ul style="list-style-type: none"> <li>• transient or continuous release</li> <li>• positively buoyant dispersions</li> <li>• neutrally buoyant dispersions</li> <li>• dense gas dispersions</li> </ul>	<ul style="list-style-type: none"> <li>• meteorological               <ul style="list-style-type: none"> <li>- wind speed</li> <li>- atmospheric stability</li> </ul> </li> <li>• topological stability               <ul style="list-style-type: none"> <li>- ground slope</li> <li>- roughness</li> <li>- obstructions</li> </ul> </li> </ul>
MODELS <ul style="list-style-type: none"> <li>• Sutton model</li> <li>• Pasquill-Gifford model</li> <li>• Box, Top-hat and variant models for dense gases</li> </ul>	<ul style="list-style-type: none"> <li>• wind               <ul style="list-style-type: none"> <li>- direction</li> <li>- speed</li> <li>- turbulence</li> <li>- persistence</li> </ul> </li> <li>• toxic load on receptors               <ul style="list-style-type: none"> <li>- breathing rate</li> <li>- exposure time</li> </ul> </li> </ul>

Note that for the degree of dispersion, the geography of the area as well as the conditions in the atmosphere are important. In terms of final impact on people or animals the exposure time, breathing rate and gas concentration will determine the toxic load.

### 6.8.3 Dispersion Modelling

In attempting to predict downwind gas concentrations many models have been developed. These models essentially fall into two major groups:

- neutrally buoyant models based on the Pasquill-Gifford model
- dense gas models based on box or top-hat representations.

Within both groups there are two basic models which account for continuous releases and also transient releases.

#### 6.8.3.1 *Positively buoyant models*

Positive buoyancy occurs when either the released gas is above atmospheric temperatures or is of a formula weight below that of air. This is the case with such gases as hydrogen ( $H_2$ ) and methane ( $CH_4$ ). Hot stack gases and other process gases can act in a positively buoyant manner.

For stack gases, that are hot, plume rise models exist to predict the amount of rise above the discharge location based on both momentum and temperature. They are commonly used in predicting downwind concentrations of pollutants from stack emissions.

In the case of light hydrocarbon releases and gases such as hydrogen, computational fluid dynamics (CFD) is often the best predictive tool to employ. It is however an expensive option from both time and effort perspectives.

### 6.8.3.2 Neutrally buoyant models

#### Continuous release

In this case the predicted downwind concentration is given by a simple Gaussian model in Table 6-19.

**TABLE 6-19 GAUSSIAN MODEL FOR NEUTRALLY BUOYANT DISPERSION**

The Gaussian model for continuous dispersion is:

$$C(x, y, z; H) = \frac{Q}{2\pi u \sigma_y \sigma_z} \exp\left[\frac{-y^2}{2\sigma_y^2}\right] \left\{ \exp\left[\frac{-(H-z)^2}{2\sigma_z^2}\right] + \exp\left[\frac{-(H+z)^2}{2\sigma_z^2}\right] \right\} \quad (6.45)$$

where

$C$	= concentration downwind at location $(x, y, z)$ ( $\text{kg}/\text{m}^3$ )	$u$	= windspeed (m/s)
$Q$	= release rate ( $\text{kg}/\text{s}$ )	$x$	= downwind distance (m)
$H$	= release height (m)	$y$	= crosswind distance (m)
$\sigma_y$	= horizontal dispersion coefficient (m)	$z$	= vertical distance (m)
$\sigma_z$	= vertical dispersion coefficient (m)		

The co-ordinates  $(x, y, z)$  describe the distances downwind, crosswind and vertical from an origin at the start of the release point at ground level. This is shown in Figure 6-22 (Turner, 1994).

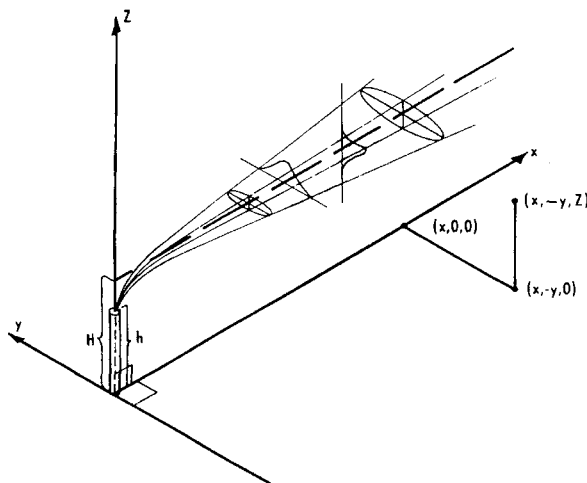


**FIGURE 6-22 CO-ORDINATE SYSTEM FOR GAS DISPERSION (Turner 1994, by permission)**

The dispersion coefficients are obtained graphically or numerically using the downwind distance and stability category of the atmosphere. This stability parameter (designated A to F) describes the degree of vertical mixing in the atmosphere. Category A describes an unstable atmosphere typical of a very sunny day. Category D is regarded as neutrally stable whilst Category F is very stable, typical of night-time conditions. The original stability categories are given in Table 6-22. It is necessary to make an assessment of the degree of insolation (solar radiation) present and note the windspeed range. It is clear that some incompatibilities exist, such that high windspeeds (> 6 m/s) with very unstable conditions like A do not normally co-exist. It is common to report stability-windspeed categories as A2 or D5 etc. Dispersion coefficients are then found from graphical presentations or from correlations such as those in Table 6-20 (CCPS 2000) for rural and urban conditions.

**TABLE 6-20 PASQUILL'S STABILITY CATEGORIES**

Surface wind speed at 10m height (m/s)	strong	Insolation moderate	slight	Night	
				thinly overcast or ≥ 4/8 cloud	≤ 3/8 cloud
< 2	A	A-B	B	-	-
2 - 3	A-B	B	C	E	F
3 - 5	B	B-C	C	D	E
5 - 6	C	C-D	D	D	D
> 6	C	D	D	D	D

**TABLE 6-21 DISPERSION PARAMETERS FOR CONTINUOUS PASQUILL-GIFFORD MODEL (CCPS, 2000)**

Pasquill-Gifford stability class	$\sigma_y$ (m)	$\sigma_z$ (m)
Rural Conditions		
A	$0.22x(1+0.0001x)^{-1/2}$	$0.20x$
B	$0.16x(1+0.0001x)^{-1/2}$	$0.12x$
C	$0.11x(1+0.0001x)^{-1/2}$	$0.08x(1+0.0002x)^{-1/2}$
D	$0.08x(1+0.0001x)^{-1/2}$	$0.06x(1+0.0015x)^{-1/2}$
E	$0.06x(1+0.0001x)^{-1/2}$	$0.03x(1+0.0003x)^{-1}$
F	$0.04x(1+0.0001x)^{-1/2}$	$0.016x(1+0.0003x)^{-1}$
Urban Conditions		
A-B	$0.32x(1+0.0004x)^{-1/2}$	$0.24x(1+0.001x)^{-1/2}$
C	$0.22x(1+0.0004x)^{-1/2}$	$0.20x$
D	$0.16x(1+0.0004x)^{-1/2}$	$0.14x(1+0.003x)^{-1/2}$
E-F	$0.11x(1+0.0004x)^{-1/2}$	$0.08x(1+0.0015x)^{-1/2}$

When the groundlevel concentration along the centreline of the plume is required, then Eq.(6.45) reduces to:

$$C(x, 0, 0; H) = \frac{Q}{\pi u \sigma_y \sigma_z} \exp\left[\frac{-H^2}{2\sigma_z^2}\right] \quad (6.46)$$

since  $y = z = 0$

The overall procedure is then to:

- select distance and release rate
- select stability category (A to F)
- determine dispersion coefficients
- obtain windspeed
- obtain release height
- calculate downwind concentration,  $C$ .

#### EXAMPLE 6-14 NEUTRALLY BUOYANT DISPERSION

A rupture occurs in an overhead line 30 m above ground releasing 2.25 kg/s of vapour that can be considered as neutrally buoyant. Moderately stable conditions with a 4 m/s breeze exist. What is the ground level concentration at a distance of 500 m downwind?

For moderately stable conditions, stability category E is selected. Dispersion coefficients from Table 6-21 under rural conditions give:

$$\sigma_y = 29\text{m} \quad \sigma_z = 13\text{m}$$

At the centreline using equation (6.46):

$$C = \frac{2.25}{\pi (29)(13)(4)} \exp \left[ -\frac{1}{2} \left( \frac{30}{13} \right)^2 \right] = 1.04 \times 10^{-4} \text{ kg} = 33 \text{ mg/m}^3$$

#### Instantaneous release

An instantaneous or transient release of gas can also be predicted. Using a Pasquill-Gifford approach the predicted downwind gas concentration is given by equation (6.47) in Table 6-24.

In this case the dispersion coefficients are somewhat different from those associated with the continuous release. It can be assumed that  $\sigma_x = \sigma_y$ . Lees (1980) quotes the dispersion coefficients as shown in Table 6-23. They are smaller than the equivalent continuous source coefficients.

**TABLE 6-22 INSTANTANEOUS GAS DISPERSION MODEL**

The Pasquill-Gifford instantaneous release model is given by:

$$C(x, y, 0; H) = \frac{2Q^*}{(2\pi)^{1.5} \sigma_x \sigma_y \sigma_z} \exp \left[ -\frac{1}{2} \left( \frac{x-ut}{\sigma_x} \right)^2 \right] \exp \left[ -\frac{1}{2} \left( \frac{H}{\sigma_z} \right)^2 \right] \exp \left[ -\frac{1}{2} \left( \frac{y}{\sigma_y} \right)^2 \right] \quad (6.47)$$

at the point  $(x, y, 0)$  i.e at ground level ( $z = 0$ ) and with a release height of  $H$

$C$	= gas concentration ( $\text{kg/m}^3$ )	$u$	= windspeed (m/s)
$Q^*$	= gas release (kg)	$t$	= time (s)
$\sigma_x$	= downwind dispersion coefficient (m)	$H$	= release height (m)
$\sigma_y$	= crosswind dispersion coefficient (m)		
$\sigma_z$	= vertical dispersion coefficient (m)		

**TABLE 6-23 DISPERSION PARAMETERS FOR INSTANTANEOUS PASQUILL-GIFFORD MODEL (Lees, 1980)**

Pasquill-Gifford stability class	$\sigma_y(\text{m})$	$\sigma_z(\text{m})$
A	$0.18x^{0.92}$	$0.60x^{0.75}$
B	$0.14x^{0.92}$	$0.53x^{0.73}$
C	$0.10x^{0.92}$	$0.34x^{0.71}$
D	$0.06x^{0.92}$	$0.15x^{0.70}$
E	$0.04x^{0.92}$	$0.10x^{0.65}$
F	$0.02x^{0.89}$	$0.05x^{0.61}$

**EXAMPLE 6-15 TANK RELEASE USING INSTANTANEOUS MODEL**

The total mass of gas released from a tank is 30 kg. The wind velocity from the north is 4 m/s and there is a stable atmosphere of category D. The effective release height is estimated at 15m. Calculate the gas concentration at 500 metres south and 20 metres west of the release, 2 minutes after the release.

Here:	$x$	= 500 m
	$y$	= 20 m
	$u$	= 4 m/s
	$Q^*$	= 30 kg

Using Table 6-23 the dispersion coefficients are:

$$\sigma_x = \sigma_y = 18\text{m}; \sigma_z = 11.6\text{m}$$

Equation (6.47) gives:

$$C(500, 100, 0; 15) = \frac{2(30)}{(2\pi)^{\frac{3}{2}}(18)(18)(11.6)} \exp \left[ -\frac{1}{2} \left( \frac{500 - (4)(120)}{18} \right)^2 \right] * \\ \exp \left[ -\frac{1}{2} \left( \frac{15}{11.6} \right)^2 \right] \exp \left[ -\frac{1}{2} \left( \frac{20}{18} \right)^2 \right] = 1.278 \times 10^{-4} \text{ kg/m}^3 = 128 \text{ mg/m}^3$$

■ ■ ■

### 6.8.3.3 Heavier than air gas dispersions

These are an important class of gas release events but their calculation requires much more sophisticated modelling procedures. A significant number of commercial packages such as DEGADIS (Dense GAs DISpersion (Spicer and Havens 1989)), HGSYSTEM (Shell 1994) or PHAST (DNV 2004) are available for these types of dispersion calculations. Some of these codes have been validated against field data in the USA and Europe.

In considering these events there are several categories of release which lead to dense gas behaviour. These include:

- (i) gases with molecular weight greater than air (29 kg/kgmole)  
e.g. LPG and chlorine.
- (ii) liquefied gases at cryogenic (below ambient) temperatures  
e.g. liquefied natural gas (LNG)
- (iii) liquefied gases under pressure with boiling point below atmospheric temperature e.g. ammonia

The release of such gases leads to a series of complex phenomena where the gas passes through a number of flow regimes. These are:

- (i) an initial buoyancy dominated flow that includes gravity spreading and air entrainment at the outer edges and the top surface.
- (ii) a stably stratified flow where the cloud is progressing along the ground but has a change in density vertically through the cloud.
- (iii) a regime of passive dispersion in the current air flow after the transition to neutrally buoyant conditions.

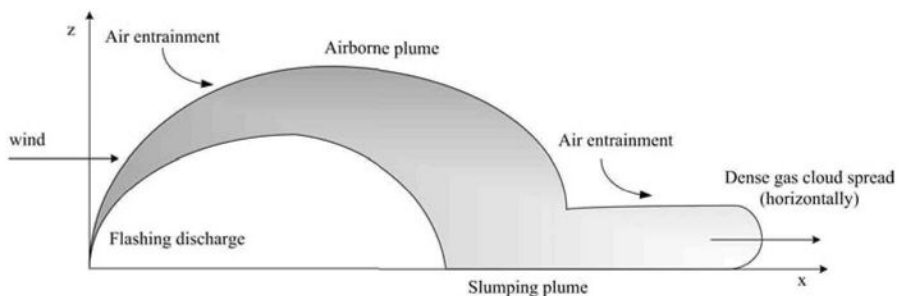


FIGURE 6-23 SCHEMATIC OF A TYPICAL HEAVY GAS RELEASE AND SPREAD

Most heavy gas dispersion models consist of a series of linked submodels. The HGSYSTEM is typical of this architecture, that addresses:

- (i) Models for the source term  
Here, submodels that predict the initial gas/liquid discharge in the form of flashing or non-flashing flows, multi-component vapour-liquid aerosols and some complex chemistry such as hydrogen fluoride releases. Pool evaporation models such as LPOOL (Cavanaugh et al. 1994) are often embedded.
- (ii) Plume models  
These track the release of materials through the stages of initial release and plume rise, the airborne trajectory followed by slumping, ground contact and subsequent gravity and wind driven cloud flow.
- (iii) Heavy gas cloud models  
These predict the gravity spreading of the cloud, the entrainment of air at the cloud surfaces, effects of heat fluxes from the ground and atmosphere. The thermodynamics of the time evolving cloud are tracked. At the point where the cloud spread leads to a passive dispersion situation, the standard Gaussian models are used to predict further dispersion.

Heavy gas models are complex tools that have their limitations. These include:

- (i) The presence of obstacles within the initial plume and subsequent cloud path. These situations require other approaches such as CFD methods.
- (ii) The presence of complex terrain, such as hills, valleys and sloping ground that cannot normally be handled by current heavy gas models.
- (iii) Wind shifts often occur and these have effects such as “steering” the dispersion. Most models do not account for this.

When such limitations exist, then either customization of existing codes are required or CFD models can be used (Havens and Spicer 2002). Evenso, there are still significant issues to address and CFD is not a “silver bullet” for these situations. The experience with CFD heavy gas models and their validation is quite variable (McBride et al. 2001) and specialized ultra low speed (ULS) wind tunnels are providing reliable data for validation purposes (Havens and Spicer 2002).

The recent work on heavy gas CFD models suggest that flat terrain models can produce results that over-estimate hazard ranges by a factor of 5 and predicted directions can vary by up to 90°. Complex terrain, such as ditches can in fact provide areas of gas concentration increases above predictions of flat terrain models. Hence it is necessary to consider the use of appropriate, validated tools specific to the task.

Heavier than air gases that form acid mists by reacting with atmospheric humidity (e.g. sulphur trioxide, hydrogen chloride) pose interesting problems in gas dispersion. Unlike heavy gases that slump to ground, reactive gases form microscopic size aerosol mists, which tend to be suspended in air. Therefore, these water reactive gases are generally modelled as neutrally buoyant gases.

### 6.8.3.4 Free turbulent jets

Free turbulent jets of gas into still air are one of the most common source terms in incident modelling. They arise from gasket, flange or pipeline component failures as well as from vessels and their attachments. The turbulent jet can be characterized by a 3 stage development, as seen in Figure 6-24. This involves:

- (i) Zone (1) near the gas orifice where a gas core exits into the ambient air, with some initial air entrainment at the orifice. If flashing liquids are released, then this is the zone where flashing occurs due to rapid pressure reduction. This is the depressurization zone which occurs within about 5 diameters of the discharge point.
- (ii) Zone (2) where significant air entrainment occurs with gas being mixed with air so that the core disappears. The lateral gas concentration goes from a 'top hat' to a Gaussian profile.
- (iii) Zone (3) represents the fully developed flow of the jet with typical Gaussian profile. This is a zone where eddy-dominated flow occurs. Both jet velocity and concentration profiles are Gaussian.

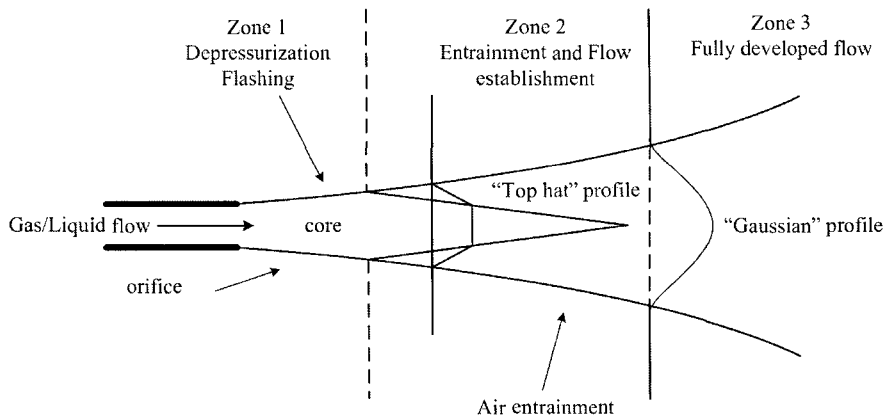


FIGURE 6-24 TURBULENT FREE JET DEVELOPMENT ZONES

A large amount of research has been done on many models. Various models are embedded within software systems such as FRED (Shell 2004), PHAST (DNV 2004) and EFFECTS (TNO 2004).

The shape of the jet is determined largely by the orifice shape and the presence of any obstacles. The jet density has an effect on the final behaviour of the flow field with light, neutral and heavy gases behaving quite differently. Wind effects are very important and greatly affect the interaction of the jet within the environment as the momentum effects dissipate.

Free jets of flammable or toxic materials are of interest because their interaction within the ambient conditions determines in the case of flammable materials the distance to the lower flammability limit (LFL). This is an indicator of hazard zones for fire events. In the case of toxics, the key factor is the



concentration profile along the jet axis and then the subsequent dispersion of the gas into the environment.

The models used to estimate temperature and concentration profiles in the turbulent jet can be of two main types:

- (i) Characteristics based on relatively simple correlations involving distribution constants that are specific to each gas. They depend on the gas to air relative density (Ricou and Spalding 1961). These distribution constants are then used to estimate the concentration and velocity distribution in any plane perpendicular to the jet axis at a distance from the orifice. They are useful, quick techniques to generate initial concentration profiles or isopleths.
- (ii) Models based on solving the conservation balances for momentum, mass, species and energy for the system. These are fundamental, mechanistic methods that can also account for directional discharge aspects as well as wind effects. One such model is JINX (Cooper 2001) whilst others such as AEROPLUME (Shell 2004) and the Unified Dispersion Model (UDM) of DNV (Holt and Witlox 2000) are embedded into larger software systems.

In most cases, these fundamental free turbulent jet models are restricted to applications where there are no nearby obstacles or direct ground interaction in the case of downward facing releases. Some work by Cooper (2001) reports on model developments to handle jet grounding, interaction with obstacles such as pipes, storage vessels, steelwork and floors. Interactions effectively change entrainment rates and hence dilution as well as impose flow resistances. Further validation work to resolve the submodels is required.

In complex geometry situations such as off-shore installations and on-shore facilities, CFD codes can be used to improve flow-field predictions. The CFD dispersion model can be used to determine the volume of module filled by flammable gas cloud in offshore facilities, which can form an input to explosion CFD model. This approach has its own limitation in that the gas dispersion CFD models have not been fully validated for the congested environment. Research continues in this area.

#### **6.8.3.5 Dispersion of fire plumes**

It is not only the thermal radiation effects of fires that need to be considered in consequence analysis but in many cases the effects of fire plume dispersion, especially where toxic compounds exist in the fire plume. This is a very common occurrence in industrial and commercial fires, especially in the case of warehouse fires that contain flammable and combustible liquids and Class 6 substances such as pesticides, herbicides and poisons. The cocktail can be lethal and in the case of unrestricted fires a number of key factors come into play. These include:

- (i) The substances in the fire
- (ii) The degree of combustion of the major substances
- (iii) The fire size (diameter) and energy release as convective heat

- (iv) The atmospheric conditions such as windspeed, relative humidity, atmospheric stability and ambient temperature.
- (v) The presence of nearby buildings
- (vi) The release location (indoors, outdoors)

#### EXAMPLE 6-16 PLANT AND WAREHOUSE FIRES

- In October 1987, 25,000 people were evacuated from surrounding areas to a chemical storage warehouse in Nantes, France. This followed a warehouse fire in the building which contained large amounts of fertilizers. Combustion gases in the fire plume included chlorine, ammonia, nitric acid and nitrogen oxides. The subsequent contaminated fire water found its way into the river Loire.
- A fire and explosion at a pesticide packaging plant in Arkansas, USA in November 1998 caused the deaths of 3 firemen and injured a further 16. A large quantity of azinphos-methyl caught fire and exploded. The fire generated a large plume which spread over the plant and surrounding area.

One of the biggest challenges in determining impacts from fire plumes is the level of combustion products in the plume. A number of workers have sought to quantify combustion products under various conditions of oxygen availability. The product spectrum can change significantly if the fire is starved of oxygen. Two significant European studies have addressed aspects of this including:

- The Combustion of Chemical Substances and the Impact on the Environment of Fire Products (EU/STEP CT91-0109)
- Guidelines for Management of Fires in Chemical Warehouses (EU/EV5V-CT93-0275)

These projects obtained data for identification and quantification of fire products. Nelson (2000) provides a summary of the projects. Other workers such as Smith-Hansen and Jorgensen (1992, 1993) did microscale combustion experiments on a wide range of pesticides, fertilizers and polymers.

Christensen et al. (1993) and Christensen (1994) addressed ammonium nitrate combustion products and pesticides combustion. The most recent studies by Costa et al. (1999) described the combustion products from over 100 substances covering plastics, fabrics, chemicals and pesticides, whilst Vinkelsoe and Johansen (2000) did small scale experiments on chlorinated pesticides, PVC and other chemicals.

All these studies provide important source data when considering the generation of fire products from a range of scenarios.

The mechanisms active in fire plume generation and subsequent dispersion are complex. The predominant mechanism is the buoyancy of the plume generated by convective heat from combustion. In most cases the convective to radiative contributions from the heat of combustion exceeds a 2 to 1 ratio. Hence there is a strong upward lift of smoke as well as unburnt substances and combustion products that subsequently interacts with the ambient conditions. On calm days fire plumes rise vertically with virtually no ground level concentration of combustion products near the fire. Strong winds deflect the buoyant plume and through convection and dispersion create, what could be, dangerous ground level concentrations of toxic

substances. The strong buoyancy driven flow, entrains large amounts of ambient air that cools and slows the vertically rising plume.

Early work on plume rise by Morton et al. (1956) has been complemented by many other authors (Porch et al. 1986, 1988; Zonato et al. 1993). Plume rise concepts are well understood and convincing models are available.

Carter (1989) combined fire dynamics with a Gaussian plume model to estimate downwind concentrations of products for both open-air and warehouse situations. In this case the Gaussian dispersion coefficients were modified to account for building wake. Plume centreline estimates were based on the Moore model (1980) excluding the momentum effects of the plume discharge. This model provided a “first estimate” tool for assessing warehouse fire impacts. Plume height is known to vary as  $x^{2/3}$  with  $x$  being the downwind distance.

Along with modelling studies, Hall and co-workers (1995, 1998) carried out extensive wind tunnel testing of many scenarios related to fire plume dispersion from warehouses where there was partial roof opening to full roof openings or no roof. What is clear from these wind tunnel experiments is that:

- (i) Ground level concentrations are a strong function of the buoyancy flux (related to convective heat release) which dominates fire events
- (ii) Plume “lift-off” from the ground is strongly influenced by the ambient windspeed and occurs when the Briggs lift-off criterion of  $L_p$  exceeds a value around 29. This corresponded to a buoyancy flux ( $F/u^3L$ ) of 0.11 where  $F$  is proportional to the fire heat output,  $u$  is the reference windspeed and  $L$  is the building height. Above 0.11 the plume lifts off into the air and ground level concentrations rapidly decrease.
- (iii) Building shape plays an important role in determining downwind ground-level concentrations.
- (iv) The number and type of openings in the roof affects downwind concentrations. More openings increase heat output through better fire ventilation and thus give higher buoyancy to plume.
- (v) The wind angle to the building is an important factor.
- (vi) Concentrations at ground level, downwind beyond the building wake, typically reduce as  $x^{-0.8}$ .

These complex factors make specific predictions of ground level concentrations extremely challenging. This is especially the case where nearby upstream and downstream buildings are present. In these cases, it is possible to use sophisticated CFD modelling (Ward 2004) or to use Gaussian models with modified dispersion coefficients that account for building geometry such as ADMS (Carruthers et al. 1999).

For situations where nearby building effects are important only CFD models provide any real chance of predicting the complex flow fields. What is clear is that one needs appropriate, validated models to carry out these predictions and that the source terms need to be carefully considered. Sensitivity studies are vital in checking output variations to source term changes and also the stage of the fire: whether initial, developing or fully developed due to the significant impact of buoyancy effects on ground level toxic concentrations.

## 6.9 REVIEW

Effects modelling is a vital part of risk management. It provides key information to a range of stakeholders that include designers, operators, emergency response personnel, town planners and government agencies. Effects modelling has reached a maturity over the last 20 years, with further validation from full-scale experiments providing valuable data for checking model predictions.

There is a growing trend in model development to address the non-standard situations through advanced computational methods such as CFD. This is particularly the case in congested situations such as off-shore platforms where complex geometries often defeat simplistic approaches to gas release, fire and explosion events.

Despite the significant advances which have reduced variability and uncertainty, sensitivity analyses are mandatory where effects can be significant on sensitive receptors (Quelch and Cameron 1994).

The fundamental chemistry of many events is still poorly understood, especially in reactive chemical events. Here, significant effort is evident in improving insights and understanding the phenomena. Software tools in the general area of effects prediction need to be used cautiously with underlying assumptions being fully appreciated.

## 6.10 REFERENCES

- American Petroleum Institute (API) 1997, *Guide for Pressure Relieving and Depressurizing Systems*, 4<sup>th</sup> edn, API RP-521, American Petroleum Institute, USA.
- Baker, Q.A., Tang, M.J., Scheier, E.A. and Silva, G.J. 1996, 'Vapour cloud explosion analysis', *Process Safety Progress*, vol. 15, no. 2, pp. 106-109.
- Bjerketvedt, D., Bakke, J.R. and Van Wingerden, K. 1997, 'Gas explosion handbook', *Journal of Hazardous Materials*, vol. 52, no. 1, pp. 1-150.
- Brasie, W.C. and Simpson, D.W. 1968, 'Guidelines for estimating damage from explosion', *Chemical Engineering Progress Loss Prevention*, vol. 2, pp. 91.
- Bull, D.C. 2004, *A critical review of post Piper-Alpha developments in explosion science for the off-shore industry*, HSE Research Report #89, HMSO, Norwich, UK.
- Carruthers, D.J., McKeown, A.M., Hall, D.J. and Porter, S. 1999, 'Validation of ADMS against wind tunnel data of dispersion from chemical warehouse fires', *Atmospheric Environment*, vol. 33A, pp. 1937-1953.
- Carter, D.A. 1989, 'Methods for estimating the dispersion of toxic combustion products from large fires', *Chemical Engineering Research and Design*, vol. 67, pp. 348-352.
- Cavanaugh, T.A., Siegel, J.H. and Steinberg, K.W. 1994, 'Simulation of vapour emissions from liquid spills', *Journal of Hazardous Materials*, vol. 38, pp. 41-63.
- CCPS 2000, Center for Chemical Process Safety, *Guidelines for Chemical Process Quantitative Risk Analysis*, 2<sup>nd</sup> edn, AIChE, New York.
- Chamberlain, G.A. 1987, 'Developments in design methods for predicting thermal radiation from flares', *Institution of Chemical Engineers Chemical Engineering Research Development*, vol. 65, pp. 299-309.

- Christensen, V., Kakko, R. and Koivisto, R. 1993, 'Environmental impact of a warehouse fire containing ammonium nitrate', *Journal of Loss Prevention in the Process Industries*, vol. 6, pp. 233-239.
- Christensen, V. 1994, 'Combustion of some pesticides and evaluation of the environmental impact', *Journal of Loss Prevention in the Process Industries*, vol. 7, pp. 39-48.
- Cook, D.K., Fairweather, M., Hammonds, J. and Hughes, D.J. 1987, 'Size and Radiative Characteristics of Natural Gas Flares. Part 1 – Field Scale Experiments, and Part 2 – Empirical Model', *Chemical Engineering Research Development*, vol. 65, pp. 310-325.
- Cooper, M.A. 2001, *A Model for jet dispersion in a congested environment*, HSE Contract Research Report 396/2001, HMSO, Norwich, UK.
- Costa, C., Treand, G., Moineault, F. and Gustin, J.L. 1999, 'Assessment of the thermal and toxic effects of chemical and pesticide pool fires based on experimental data obtained using the Tewarson apparatus', *Process Safety and Environmental Protection*, vol. 77B, pp. 154-164.
- Crowley, L.T. and Johnson, A.D. 1992, *Oil and Gas Fires: Characteristics and Impacts*, Research Report Offshore Technology Information, OTI92 596, HSE, UK.
- Crowley, L.T. 1992a, *Behaviour of Oil and Gas fires in the presence of confinement and obstacles*, Research Report, OTI92 597, HSE, UK.
- Crowley, L.T., 1992b, *Current fire research: experimental, theoretical and predictive modelling resources*, Res. Report OTI 92 598, HSE, UK, vol. 1.
- Daesim 2004, *Daesim Studio: Risk Assessor*, Daesim Technologies Pty Ltd, Australia, Available at: <http://www.daesim.com/>.
- DNV 2004, *PHAST - Process Hazard Analysis Software Tool*, DNV Software, Available at: <http://www.dnv.com/software/>.
- Fire and Blast Information Group (FABIG) 1988, *Blast and Fire Engineering Projects for Topside Structures*, Steel Construction Institute, UK. Available at: <http://www.fabig.com>.
- Fletcher, B. and Johnson, A.E. 1984, *The Discharge of Superheated Liquids from Pipes*, Institution of Chemical Engineers, Rugby, UK.
- Guilbert, P.W. and Jones, I.P. 1996, *Modelling of Explosions and Deflagrations*, HSE Contract Research Report 93/1996, HMSO, UK.
- Hall, D.J., Kukadia, V., Walker, S. and Marsland, G. 1995, *Plume dispersion from chemical warehouse fires*, Technical Report, Building Research Establishment, Garston, Watford WD2 7JR, United Kingdom.
- Hall, D.J., Kukadia, V., Walker, S. and Marsland, G.W. 1998, 'Deposition of large particles from warehouse fire plumes—A small-scale wind tunnel model study', *Journal of Hazardous Materials*, vol. 59, pp. 13-29.
- Hamins, A., Kashiwagi, T. and Buch, R. 1995, 'Characteristics of Pool Fire Burning', *Fire Resistance of Industrial Fluids*, ASTM STP 1284, American Society for Testing Materials, Philadelphia, USA.
- Havens, J. and Spicer, T. 2002, 'New models predict consequences of LNG Releases', *GasTIPS*, Fall 2002, Gas Technology Institute, USA.
- Hawksley, J.L. 1986, 'Unconfined vapour cloud explosions involving hydrogen rich gases - estimating the blast effects', *Loss Prevention Bulletin*, no. 68, The Institution of Chemical Engineers, Rugby, UK.
- Holman, J.P. 1981, *Heat Transfer*, 5<sup>th</sup> edn, McGraw-Hill, USA.

- Holt, A. and Witlox, H.W.M. 2000, *Validation of the Unified Dispersion Model*, DNV Software-Risk Management, Consequence Modelling Documentation, UDM6.0, London, UK.
- Johnson, A.D., Shirvill, L.C. and Ungut, A. 1999, *CFD Calculation of Impinging Gas Jet Fires*, Offshore Technology Report OTO1999011, HSE, UK.
- Johnson, A.D., Brightwell, H.M. and Carsley, A.J. 1994, 'A model for predicting the thermal radiation hazards from large-scale horizontally released natural gas jet fires', *Transactions of Institution of Chemical Engineers*, Process Safety and Environmental Protection, vol. 72 Part B, pp. 157-166.
- Johnson, A.D. 1992, 'A model for predicting thermal radiation hazards from large-scale pool fires', *Institution of Chemical Engineers Symposium Series No. 130*, pp. 507-524.
- Kawaramura, P.I. and Mackay, D. 1987, 'The evaporation of volatile liquids', *Journal of Hazardous Materials*, vol. 15, pp. 365-376.
- Kinsella, K.G. 1992, 'A Rapid Assessment Methodology for the Prediction of Vapour Cloud Explosion Overpressure', *International Conference on Safety and Loss Prevention*, Singapore.
- Lawrence, F.E. and Johnson, E.E. 1974, 'Design for limiting explosion damage', *Chemical Engineering*, vol. 7, January.
- Lea, C.J. and Ledin, H.S. 2002, *A Review of the State-of-the-Art in Gas Explosion Modelling*, Health and Safety Laboratory Report HSL/2002/02, Fire and Explosion Group, Buxton, UK.
- Lees, F.P. 1980, *Loss Prevention in the Process Industries*, 1<sup>st</sup> edn, Butterworths, UK.
- Lees, F.P. 2001, *Loss Prevention in the Process Industries*, 2<sup>nd</sup> edn, Butterworths-Heinemann, Oxford, UK.
- McBride, M.A., Reeves, A.B., Vanderheyden, M.D., Lea, C.J. and Zhou, X.X. 2001, 'Use of advanced techniques to model the dispersion of chlorine in complex terrain', *Transactions of Institution of Chemical Engineers*, vol. 79, Part B, pp. 89-102.
- Mercx, W.P.M., van den Berg, A.C. and van Leeuwen, D. 1998, *Application of correlations to quantify the source strength of vapour cloud explosions in realistic situations: Final report for the project 'GAMES'*, TNO Report, PML1998-C53, Rijswijk, The Netherlands.
- Mercx, W.P.M., van den Berg, A.C., Hayhurst, C.J., Robertson, N.J. and Moran, K.C. 2000, 'Developments in vapour cloud explosion blast modelling', *Journal of Hazardous Materials*, vol. 71, pp. 301-319.
- Moore, D.J. 1980, 'Lectures on plume rise' in *Atmospheric Planetary Boundary Layer Physics, Developments in Atmospheric Science*, ed. A. Longhetto, Elsevier, Amsterdam, pp. 327-354.
- Morton, B.R., Taylor, G. and Turner, J.S. 1956, 'Turbulent, gravitational convection from maintained and instantaneous sources', *Proceedings of the Royal Society*, vol. 234, pp. 1-23.
- Nelson, G.L. 2000, 'Fire and pesticides: A review and analysis of recent work', *Fire Technology*, vol. 36, no. 3, pp. 163-183.
- National Fire Protection Association. *Flammable and Combustible Liquid Codes*, National Fire Protection Association, Quincy, Massachusetts. NFPA 30:2000.
- Peress, J. 2003, 'Estimate Evaporative Losses from Spills', *Chemical Engineering Progress*, April, pp. 32-34.

- Popat, N.R., Catlin, C.A., Arntzen, B.J., Lindstedt, R.P., Hjertager, B.H., Solberg, T., Saeter, O. and van den Berg, A.C. 1996, 'Investigations to improve and assess the accuracy of computational fluid dynamic based explosion models', *Journal of Hazardous Materials*, vol 45, pp.1-25.
- Porch, M., Stout, J.E., Cermak, J.E. and Peterka, J.A. 1986, *Physical Modeling of Large-area Fire Plumes*, Technical Report DNA-TR-85-364, Colorado State University, USA.
- Porch, M. and Cermak, J.E. 1988, 'Scale-model simulations of large area fire plumes', *International Symposium on Scale Modeling*, July 18-22, Tokyo, Japan, Japan Soc. Mech. Engineers.
- Pritchard, M.J. and Binding, T.M. 1992, 'FIRE2: a new approach for predicting thermal radiation levels from hydrocarbon pool fires', *Institution of Chemical Engineers Symposium Series No. 130*, pp. 491-505.
- Quelch, J. and Cameron, I.T. 1994, Uncertainty representation and propagation in QRA using fuzzy sets, *Journal of Loss Prevention in the Process Industries*, vol. 7, no. 6, pp. 463-473.
- Rew, P.J. and Hulbert, W.G. 1996, *Development of pool fire thermal radiation model*, HSE Contract Research Report 96/1996, HSE, London, HMSO, ISBN 07176 10845.
- Ricou, F.P. and Spalding, B.D. 1961, 'Measurement of entrainment by axisymmetrical turbulent jets', *Journal of Fluid Dynamics*, vol. 11, pp. 21-32.
- Shaw, P. and Briscoe, F. 1978, *Evaporation from Spills of Hazardous Liquids on Land and Water*, UK Atomic Energy Authority Safety and Reliability Directorate, Culcheth, Warrington.
- Shell 2004, *FRED - Fire, Release, Explosion and Dispersion*, Shell Global Solutions, Available at:  
<http://www.shellglobalsolutions.com/hse/software/fred.htm>.
- Shell 1994, *HGSYSTEM - Heavy Gas System V3.0*, Shell Internationale Research Maatschappij B.V., The Netherlands. Available at: <http://www.hgsystem.com/> ,
- Smith-Hansen, L. and Jorgensen, K.L. 1992, *Combustion of Chemical substances and the impact of the environment of the fire products: Microscale experiments*, Technical Report, Risø National Laboratory, Roskilde, Denmark.
- Smith-Hansen, L. and Jorgensen, K.L. 1993, 'Characterization of fire products from organophosphorus pesticides using the DIN 53436 method', *Journal of Loss Prevention in the Process Industries*, vol. 6, pp. 227-232.
- Spicer, T. and Havens, J. 1989, *User's Guide for the DEGADIS 2.01 Dense Gas Dispersion Model*, Report EPA-450/4-89-019, USEPA, USA.
- Standards Australia. *The Storage and Handling of Flammable and Combustible Liquids*, Standards Australia, AS 1940:1993.
- Tang, M.J. and Baker, Q.A. 2000, 'Comparison of blast curves from vapour cloud explosions', *Journal of Loss Prevention in the Process Industries*, vol. 13, pp. 433-438.
- TNO 1992, *Methods for the Calculations of Physical Effects*, Yellow Book 2<sup>nd</sup> edn, CPR 14E, Director General of Labour, Voorburg, The Netherlands.
- TNO 1997, *Methods for the Calculation of Physical Effects*, Yellow Book 3<sup>rd</sup> edn, CPR14E Part 1, Director-General for Social Affairs & Employment, The Netherlands.

- TNO 2004, *EFFECTS - Calculating the physical effects due to hazardous material releases*, TNO Environment and Industrial Safety, Available at: <http://www.mep.tno.nl/software/>.
- Thomas, P.H. 1963, 'The size of flames from natural fires', *9<sup>th</sup> Int'l Combustion Symposium*, Combustion Institute, Pittsburgh, USA, pp. 844.
- Turner, D.B. 1994, *Workbook of Atmospheric Dispersion Estimates - An Introduction to Dispersion Modeling*, 2<sup>nd</sup> edn, Lewis Publishers, ISBN1-56670-023-X.
- van den Berg, A.C., 1985, 'The Multi-Energy Method - a framework for vapour cloud explosion blast prediction', *Journal of Hazardous Materials*, vol. 12, pp. 1-10.
- van den Berg, A.C., van Wingerden, C.J.M. and The, H.G. 1991, 'Vapour Cloud Explosions: Experimental investigation of key parameters and blast modelling', *Transactions of IChemE.*, Part B, vol. 69, pp. 139-148.
- Vikelsoe, J. and Johansen, E. 2000, 'Estimation of dioxin emission from fires in chemicals', *Chemosphere*, vol. 40, pp. 165-175.
- Ward, A. 2004, *Application of Computational Fluid Dynamics to Modelling the near-field, atmospheric dispersion of combustion products in chemical warehouse fires*, PhD thesis, School of Engineering, The University of Queensland, Brisbane.
- Wells, G.L. 1980, *Safety in Process Plant Design*, George Godwin Ltd, London, ISBN 0-7114-5506-6.
- Zonato, C., Vidili, A., Pastorino, R and De Faveri, D.M. 1993, 'Plume rise of smoke coming from free burning fires', *Journal of Hazardous Materials*, vol. 34, pp. 69-79.

## 6.11 NOTATION

AEROPLUME	Jet release model in HYSYSTEM
API	American Petroleum Institute
AS	Australian Standard
AutoReaGas	CFD explosion code by TNO/Century Dynamics
bar	Pressure unit (1 bar = 100 kPa)
BLEVE	Boiling liquid expanding vapour explosion
CCPS	Center for Chemical Process Safety
CFD	Computational fluid dynamics
CFX	General purpose CFD code, AEA Technology, UK
C:H	Carbon to hydrogen ratio
CH <sub>4</sub>	Methane
CO	Carbon monoxide
CO <sub>2</sub>	Carbon dioxide
COBRA	CFD explosion code, Mantis Numerics, UK
DEGADIS	Dense GAs DISpersion
EFFECTS	TNO effects software (The Netherlands)
EXSIM	CFD explosion code by Tel-tek and Shell Global Solutions
FABIG	Fire and Blast Information Group
FLACS	Flame acceleration simulator, CMRI Norway
FRED	Fire, release, explosion, dispersion software (Shell)
H <sub>2</sub>	Hydrogen



HF	Hydrogen fluoride
HGSYSTEM	Heavy gas system (Shell)
HSE	Health & Safety Executive, UK
JINX	Jet dispersion model (Advantica Ltd, UK)
K	Kelvin
kg	kilograms
kJ	kilo-Joules
kPa	kilo-Pascals
kW	kilo-Watts
LFL	Lower flammability limit
LNG	Liquefied natural gas
LPG	Liquefied petroleum gas
LPOOL	Liquid pool model (Exxon Research and Engineering)
m	metres
m <sup>2</sup>	square metres
m <sup>3</sup>	cubic metres
MEM	Multi-energy model
MERGE	EU project on
mg	milligrams
mm	millimetres
MPa	Mega Pascal
N <sub>2</sub>	Nitrogen
NFPA	National Fire Protection Association
O <sub>2</sub>	Oxygen
Pa	Pascals
PEMEX	Petróleos Mexicanos, Mexico
PETN	Pentaerythritoltetranitrate
PHAST	Process hazard analysis software tool (Det Norske Veritas)
RDX	Cyclo-trimethylene-trinitramine explosive
RH	Relative humidity
s	seconds
SIS	Safety instrumented systems
TNO	The Netherlands Organization for Applied Scientific Research
TNT	Trinitro-toluene
UDM	Unified dispersion model
ULS	Ultra low speed
VBR	Volume blockage ratio
VCE	Vapour cloud explosion